

Neutrinoless $\beta\beta$ -Decay in DCEQTDA

C. De Conti¹, V. dos S. Ferreira^{2,3}, A.R. Samana², C.A. Barbero^{4,5} and F. Krmpotić⁴

¹São Paulo State University (UNESP), School of Engineering and Sciences, 19274-000 Rosana, SP, Brazil.

²Departamento de Ciências Exatas, Universidade Estadual de Santa Cruz, Campus Soane Nazaré de Andrade, Rod. Jorge Amado Km 16, 45662-900 Ilhéus, BA, Brazil.

³Centro de Ciências Exatas e Tecnológicas, Universidade Federal do Recôncavo da Bahia, 44380-000 Cruz das Almas, BA, Brazil.

⁴Departamento de Física, Universidad Nacional de La Plata, C.C. 67, 1900 La Plata, Argentina.

⁵Instituto de Física La Plata, CONICET, 1900 La Plata, Argentina.

Abstract

We have recently developed a nuclear model, which is a natural extension of the pn -QRPA model, specially designed to describe double charge exchange (DCE) processes generated by two-body DCE transition operators. It is based on the Quasiparticle Tamm-Dancoff Approximation (QTDA) for pn and $2p2n$ excitations in intermediate and final nuclei, respectively, and will be called DCEQTDA. As such, this model, having the same number of free parameters as the pn -QRPA, also brings into play the excitations of four quasiparticles to build up the final nuclear states, which are then used to evaluate the nuclear matrix elements (NMEs) for all 0^+ and 2^+ final states, including resonances, and not just for the ground state as in pn -QRPA. In addition, it allows us to evaluate: (a) the values of $Q_{\beta\beta}$, (b) the excitation energies in final nuclei, and (c) the DCE sum rules, which are fulfilled in the DCEQTDA. So far, this model has been used mainly to calculate double beta decays with the emission of two neutrinos ($2\nu\beta\beta$ -decay). Here, we extend it to the study of these processes when no neutrinos are emitted ($0\nu\beta\beta$ -decay), evaluating them in a series of nuclei, but paying special attention to (i) ^{76}Se , which

have been measured recently in the GERDA and MAJORANA experiments, and (ii) ^{124}Te , for which the first direct observation of the double electron capture 2ν has been performed with the XENON1T dark matter detector. We obtain good agreement with the data for both the ground state and the excited states. The validity of the DCEQTDA model is checked by comparing the calculation with the experimental data for the $2\nu\beta\beta$ NMEs, and for the $Q_{\beta\beta}$, in a series of nuclei.

Keywords: neutrino-nucleus, nuclear structure, QRPA

1 Introduction

If the driving mechanism of the $0\nu\beta\beta$ -decay is through the exchange of a left-handed light neutrino of Majorana type, which is forbidden in the Standard Model, its detection will allow us to find the effective mass of the neutrino $\langle m_\nu \rangle$, provided we know the nuclear matrix element (NME) $M^{0\nu}$, since the decay amplitude rate is proportional to $|\langle m_\nu \rangle M^{0\nu}|^2$.

These NMEs are calculated using different nuclear models, and there are no experimental data or model-independent sum rules to corroborate their calculated values. As a consequence, a large scatter in the results (up to factors of three) has emerged.

Strictly speaking, despite the enormous efforts invested in these calculations, we are still not entirely sure of the order of magnitude of the NMEs $M^{0\nu}$ [1]. We also do not know what is the total transition intensity of the $0\nu\beta\beta$ -decay, and what is the proportion of it that ends into the ground state. We will try to give an answer to these questions. We know this only for the double Gamow-Teller operator from the work of Auerbach *et al.* [2–5], but not for $M^{0\nu}$.

In recent years much attention has been paid to $\beta\beta$ -decays to excited states in final nuclei, operating several large underground experiments, such as the GERDA [6], MAJORANA [7], and LEGEND [8] searches in ^{76}Ge , the first two of which have already been completed.

On the other hand, the NUMEN heavy ion multidetector, designed for a complementary approach to $0\nu\beta\beta$ NMEs, is currently taking data [9–13]. Theoretical comparisons have been made [14–17] between the $0\nu\beta\beta$ NME and the double Gamow-Teller transition to the ground state of the final nucleus, where a very small portion of the total strength is found.

In addition to evaluating the $\beta\beta^-$ -decays of ^{76}Ge , we also discuss the $\beta\beta^+$ -decays of ^{124}Xe , where has been done the first direct observation of the 2ν double electron capture ($2\nu ee$) for the ground state in ^{124}Te , with the half-life $\tau_{2\nu}^{ee}(0_1^+) = (1.8 \pm 0.6) \times 10^{22}$ y [18], which is the longest half-life ever measured directly, about one trillion times the age of the Universe¹. More recently, by a XMASS experiment [19] has been imposed the constraint on this half-life $\tau_{2\nu}^{ee}(0_1^+) > 2.1 \times 10^{22}$ y at 90% confidence level, which is consistent with above measurement.

2 General Formalism for DCE Processes

2.1 Single and Double Charge Exchange Strengths and their Sum Rules

The Single Charge Exchange (SCE) operators $\mathcal{O}_0^\mp = \tau^\mp$, and $\mathcal{O}_1^\mp = \tau^\mp \sigma$, play a fundamental role in β^\mp -decays: $(A, Z) \rightarrow (A, Z \pm 1)$. In the same way, the Double Charge Exchange (DCE) operators $\mathcal{D}_{J\mathcal{J}}^\mp = [\mathcal{O}_J^\mp \times \mathcal{O}_{\mathcal{J}}^\mp]_{\mathcal{J}}$, with $J = 0, 1$,

¹As pointed out by Doi [20] in order to satisfy the energy-momentum conservation this decay mode should be accompanied by an emission of some additional particle(s).

and $\mathcal{J} = 0, 2$, are essential for the $\beta\beta^\mp$ -decays: $(A, Z) \rightarrow (A, Z \pm 2)$, and closely related to the 0ν and 2ν NMEs. In turn, the operators \mathcal{O}_J , and \mathcal{D}_{JJ}^\mp are related to the corresponding SCE, and DCE reaction processes, and their giant resonances.

An attempt is made to infer the value of $M^{0\nu^-}(0_1^+)$ from heavy-ion reaction data at low momentum transfer using M_{10} and M_{00} for $M_A^{0\nu}$ and $M_V^{0\nu}$, respectively ², although these two sets of NMEs differ from each other in several respects, as will be discussed below.

The one-body matrix elements matrix elements are usually expressed as

$$\langle J_i^+ || \mathcal{O}_J^\pm || 0^+ \rangle = \sum_{pn} \rho^\pm(pn, J_i^\pi) W_{J0J}(pn), \quad (1)$$

and

$$\langle \mathcal{J}_f^+ || \mathcal{O}_J^\pm || J_i^+ \rangle = \sum_{np} \rho^\pm(pn, J_i, \mathcal{J}_f^+) W_{J0J}(pn), \quad (2)$$

i.e., as a product of model dependent one-body densities

$$\begin{aligned} \rho^-(pn, J_i) &= \hat{J}^{-1} \langle J_i || (c_p^\dagger c_{\bar{n}})_J || 0_i^+ \rangle, \\ \rho^+(pn, J_i) &= \hat{J}^{-1} \langle J_i || (c_n^\dagger c_{\bar{p}})_J || 0_i^+ \rangle, \end{aligned} \quad (3)$$

from the initial to intermediary states, and

$$\begin{aligned} \rho^+(pn, J_i, \mathcal{J}_f) &= \hat{J}^{-1} \langle \mathcal{J}_f || (c_n^\dagger c_{\bar{p}})_J || J_i \rangle, \\ \rho^-(pn, J_i, \mathcal{J}_f) &= \hat{J}^{-1} \langle \mathcal{J}_f || (c_p^\dagger c_{\bar{n}})_J || J_i \rangle, \end{aligned} \quad (4)$$

from the intermediary to final states, and of the single-particle NMEs ³:

$$\begin{aligned} W_{LSJ}(pn) &\equiv \sqrt{4\pi} \langle p || O_{LSJ} || n \rangle \\ &= \sqrt{2} \hat{S} \hat{J} \hat{L} \hat{l}_n \hat{j}_n \hat{j}_p (l_n L | l_p) \left\{ \begin{matrix} l_p & \frac{1}{2} & j_p \\ L & S & J \\ l_n & \frac{1}{2} & j_n \end{matrix} \right\}, \end{aligned} \quad (5)$$

of the non-relativistic β -decay operators

$$O_{LSJ} = (Y_L \otimes \sigma^S)_J, \quad (6)$$

with $S = 0$ (1) for vector (axial vector) operators. Note that $O_{0JJ} \equiv O_J$, and $(l_n L | l_p) \equiv (l_n 0 L 0 | l_p 0)$.

²(See for example [21, Eq. (16)]).

³We use here the angular momentum coupling scheme $|(l_n, l_j)j\rangle$ [22].

The nuclear models are employed to evaluate the total SCE strengths

$$S_J^{\{\mp 1\}} \equiv \sum_i |\langle J_i | \mathcal{O}_J^\mp | 0^+ \rangle|^2 \equiv \sum_i s_J^{\{\mp 1\}}(J_i), \quad (7)$$

going from the initial ground state $|0^+\rangle$ to intermediate states $|J_i^+\rangle$, as well as the total DCE strengths

$$S_{JJ}^{\{\mp 2\}} = \sum_f |\langle \mathcal{J}_f | \mathcal{D}_{JJ}^\mp | 0^+ \rangle|^2 \equiv \sum_f s_{JJ}^{\{\mp 2\}}(\mathcal{J}_f), \quad (8)$$

going from $|0^+\rangle$ to final states $|\mathcal{J}_f\rangle$.

When both $|J_i\rangle$ and $|\mathcal{J}_f\rangle$ are complete sets of states that can be reached by operating with \mathcal{O}_J^\pm , and \mathcal{D}_{JJ}^\pm on $|0^+\rangle$, the strength differences

$$\begin{aligned} S_J^{\{1\}} &= S_J^{\{-1\}} - S_J^{\{+1\}}, \\ S_{JJ}^{\{2\}} &= S_{JJ}^{\{-2\}} - S_{JJ}^{\{+2\}}, \end{aligned} \quad (9)$$

should obey the SCE Ikeda's sum rules [23]

$$S_J^{\{1\}} = (2J + 1)(N - Z), \quad (10)$$

and the DCE sum rules [2, 24, 25]

$$\begin{aligned} S_{00}^{\{2\}} &= 2(N - Z)(N - Z - 1), \\ S_{10}^{\{2\}} &= 2(N - Z) \left(N - Z + 1 + 2S_1^{\{-1\}} \right) - \frac{2}{3}C, \\ S_{12}^{\{2\}} &= 10(N - Z) \left(N - Z - 2 + 2S_1^{\{-1\}} \right) + \frac{5}{3}C, \end{aligned} \quad (11)$$

where C is a relatively small positive quantity, given by [25, Eq. (4)]. Since the terms proportional to C will not be considered in the present work, the following inequalities arise:

$$S_{10}^{\{2\}} \geq S_{10}^{\{2\}}, \quad S_{12}^{\{2\}} \leq S_{12}^{\{2\}}. \quad (12)$$

It is desirable that any nuclear model used to calculate DCE processes satisfies the sum rules (11) for the total strengths $S_{JJ}^{\{\mp 2\}}$. Through them, we can evaluate the fractions of strengths going to the individual states as

$$\begin{aligned} R^{\{\mp 1\}}(J_i) &= s_J^{\{\mp 1\}}(J_i) / S_J^{\{\mp 1\}}, \\ R_{JJ}^{\{\mp 2\}}(\mathcal{J}_f) &= s_{JJ}^{\{\mp 2\}}(\mathcal{J}_f) / S_{JJ}^{\{\mp 2\}}, \end{aligned} \quad (13)$$

calibrating in this way the NMEs of the operators \mathcal{O}_J and $\mathcal{D}_{J\mathcal{J}}$. Later, the same will be done with the $0\nu\beta\beta$ NMEs, which will allow us to determine their order of magnitude.

The main difference between $(S_J^{\{1\}}, S_{J\mathcal{J}}^{\{2\}})$, and $(S_J^{\{1\}}, S_{J\mathcal{J}}^{\{2\}})$ is that while the former depend on nuclear structure the latter do not. These two quantities in principle should be equal to each other, and it is desirable that any nuclear model used to calculate the SCE and DCE processes satisfies the condition.

This generally occurs in most theoretical calculations with the Ikeda's sum rule, but not with $S_{J\mathcal{J}}^{\{2\}}$ because of (12).

When the above condition on the completeness of the basis $|J_i\rangle$ is satisfied, we get

$$\begin{aligned} \langle \mathcal{J}_f | \mathcal{D}_{J\mathcal{J}}^\mp | 0^+ \rangle &= \sum_i \langle \mathcal{J}_f^+ | \mathcal{O}_J^\pm | J_i \rangle \langle J_i | \mathcal{O}_J^\pm | 0^+ \rangle \\ &= \sum_i \sum_{p_1 n_1 p_2 n_2} \varrho^\mp(p_1 n_1 p_2 n_2; J_i, \mathcal{J}_f) W_{J_0 J}(p_1 n_1) W_{J_0 J}(p_2 n_2), \\ &\equiv \sum_i \langle \mathcal{J}_f | \mathcal{D}_{J_i \mathcal{J}}^\mp | 0^+ \rangle \end{aligned} \quad (14)$$

with $J = 0, 1$, and $\mathcal{J} = 0, 2$, and

$$\varrho^\mp(p_1 n_1 p_2 n_2; J_i, \mathcal{J}_f^+) = \varrho^\mp(p_1 n_1; J_i) \varrho^\mp(p_2 n_2; J_i, \mathcal{J}_f^+), \quad (15)$$

Given that the reaction matrix elements $\langle \mathcal{J}_f | \mathcal{D}_{J\mathcal{J}}^\mp | 0^+ \rangle$ do not depend on the energies of the intermediate $|J_i\rangle$ states, we can simplify their evaluation, using

$$\begin{aligned} M_J^\mp(\mathcal{J}_f) &\equiv \langle \mathcal{J}_f | \mathcal{D}_{J\mathcal{J}}^\mp | 0^+ \rangle = \hat{J}^{-1} \sum_{p_1 n_1 p_2 n_2} \bar{\varrho}^\mp(p_1 n_1 p_2 n_2; J \mathcal{J}_f^+) \\ &\quad \times W_{0 J J}(p_1 n_1) W_{0 J J}(p_2 n_2). \end{aligned} \quad (16)$$

where

$$\begin{aligned} \bar{\varrho}^\mp(p_1 n_1 p_2 n_2; J \mathcal{J}_f^+) &= \sum_i \varrho^\mp(p_1 n_1 p_2 n_2; J_i \mathcal{J}_f^+) \\ &\equiv \sum_i \varrho^\mp(p_1 n_1; J_i) \varrho^\mp(p_2 n_2; J_i, \mathcal{J}_f^+) \end{aligned} \quad (17)$$

2.2 Two-neutrino Double Beta Decay

The $2\nu\beta\beta$ -decay processes can occur, if energetically allowed, as a second order perturbation of the weak Hamiltonian, independently of whether neutrinos are Dirac or Majorana and massive or massless allowed [20]. Their matrix elements

read

$$M_{J_f}^{2\nu^\mp}(\mathcal{J}_f) = \frac{-g_J^2}{\hat{\mathcal{J}}} \sum_i \frac{\langle \mathcal{J}_f || \mathcal{D}_{J_i, \mathcal{J}}^\mp || 0^+ \rangle}{\left(\mathcal{D}_{J_i, \mathcal{J}_f}^{2\nu^\mp} \right)^{\mathcal{J}+1}}, \quad (18)$$

for F ($g_0 \equiv g_V$), and GT ($g_1 \equiv g_A$) transitions. Moreover, $\hat{\mathcal{J}} = \sqrt{2\mathcal{J}+1}$, and $|\mathcal{J}_f^+\rangle$ are the final states with $\mathcal{J} = 0$, and $\mathcal{J} = 2$.

The energy denominator is

$$\begin{aligned} \mathcal{D}_{J_i, \mathcal{J}_f}^\mp &= E_{J_i}^{\{\mp 1\}} - E_{0^+}^{\{0\}} + \frac{E_{0^+}^{\{0\}} - E_{\mathcal{J}_f}^{\{\mp 2\}}}{2}, \\ &= E_{J_i}^{\{\mp 1\}} - \frac{E_{0^+}^{\{0\}} + E_{\mathcal{J}_f}^{\{\mp 2\}}}{2} \end{aligned} \quad (19)$$

where $E_{0^+}^{\{0\}}$, $E_{J_i}^{\{\mp 1\}}$, and $E_{\mathcal{J}_f}^{\{\mp 2\}}$ are, respectively, the energies of: (i) the ground state of the decaying nucleus (A, Z), (ii) the J_i^+ state in the intermediate nucleus ($A, Z \pm 1$), and (iii) the \mathcal{J}_f^+ state in the final nucleus ($A, Z \pm 2$). The term $(E_{0^+}^{\{0\}} - E_{\mathcal{J}_f}^{\{\mp 2\}})/2$ comes from the approximation done for the energy of the leptons $e + \nu$, emitted in the first β decay. It is equal to half of the corresponding Q -value (see (39)).

2.3 Neutrinoless Double Beta Decay

If neutrinos are assumed to be Majorana particles, then the $0\nu\beta\beta$ -decay mode can take place under some conditions, which are explained by Doi [20].

The $0\nu\beta\beta$ NMEs for the final 0^+ and 2^+ states are completely different from each other, since they are spawned from different parts of the vector (V), and axial-vector (A) weak-hadronic-currents $J^\mu = (\rho, \mathbf{j})$; see, for instance [26, Eqs. (7), (8)]. In fact, while the first comes from ρ_V , and \mathbf{j}_A , which are velocity independent parts of J^μ (ρ_V , and \mathbf{j}_A), and are akin to \mathcal{D}_{00} , and \mathcal{D}_{10} , respectively, the second comes from the velocity dependent parts of J^μ (ρ_A , and \mathbf{j}_V), that do not resemble \mathcal{D}_{12} ; see, [27, Eqs.(5), (6)]. Because of this, $0\nu\beta\beta$ -decays to final states 2^+ are not considered here.

In the case of 0^+ final states, pseudo-scalar (P), and weak magnetism (M) induced currents also contribute to the $0\nu\beta\beta$ -decay, and the corresponding NME, $M^{0\nu^\mp}(0_f^+)$, is usually presented as a sum of F, GT, and Tensor (T) parts (see, for example, [28, Eq. (3)]). The term F arises only from the V weak current, but the GT and T terms contain mixtures of A, M, and P currents (see Refs. [22, 26, 29, 30]). We prefer to highlight the individual contributions of the weak currents, and write

$$M^{0\nu^\mp}(0_f^+) = \sum_{X=V,A,M,P} M_X^{0\nu^\mp}(0_f^+), \quad (20)$$

The weak coupling constants g_V , g_A , $f_M = (g_M + g_V)/(2M_N)$, and $g'_P = g_P/(2M_N)$ are incorporated within $M_X^{0\nu^\mp}(0_f^+)$. They are fixed as follows: $g_V = 1$, and $g_M = 3.7$ from Conservation of Vector Current, $g_A = 1.27$ from the experimental data [31], and $g_P = 2M_N g_A/(q^2 + m_\pi^2)$ from the assumption of Partially Conserved Axial Current [32].

The Finite Nucleon Size effects are introduced through the usual dipole form factors

$$\begin{aligned} g_V &\rightarrow g_V(k^2) \equiv g_V \Lambda_V^4 (\Lambda_V^2 + k^2)^{-2}, \\ g_A &\rightarrow g_A(k^2) \equiv g_A \Lambda_A^4 (\Lambda_A^2 + k^2)^{-2}, \\ f_M &\rightarrow f_M(k^2) \equiv f_M \Lambda_V^4 (\Lambda_V^2 + k^2)^{-2}, \\ g'_P &\rightarrow g'_P(k^2) \equiv g'_P \Lambda_A^4 (\Lambda_A^2 + k^2)^{-2}, \end{aligned} \quad (21)$$

where $\Lambda_V = 0.85$ GeV, and $\Lambda_A = 1.086$ GeV are the cut-off parameters as found in [33–35]. The Short Range Correlations are included in the way indicated in [30, Eqs. (2.29)-(2.31)].

We will also discuss the NMEs $M_{V_0}^{0\nu^\mp}$ and $M_{A_1}^{0\nu^\mp}$ which are the parts of $M_V^{0\nu^\mp}$ and $M_A^{0\nu^\mp}$ engendered, respectively, only by the intermediate states $J_i^\pi = 0_i^+$ and 1_i^+ .

Like the NMEs $M_J^{2\nu^\mp}(\mathcal{J}_f)$, the $M_X^{0\nu^\mp}(0_f^+)$ in (20) can be expressed by the density matrix ϱ^\mp , as follows

$$\begin{aligned} M_X^{0\nu^\mp}(0_f^+) &= \sum_{J_i} \sum_{p_1 p_2 n_1 n_2} \varrho^\mp(p_1 n_1 p_2 n_2; J_i^\pi 0_f) \\ &\times m_X^{0\nu}(p_1 n_1 p_2 n_2; J, \mathcal{D}_{J_i, 0_f}), \end{aligned} \quad (22)$$

where $m_X^{0\nu}(p_1 n_1 p_2 n_2; \mathcal{D}_{J_i, 0_f})$ are the single particle $0\nu\beta\beta$ NMEs, which do not depend on nuclear models.

Because the $0\nu\beta\beta$ NMEs depend only very weakly on the energy denominators $\mathcal{D}_{J_i^\pi, 0_f^+}$, calculations are usually performed in the Closure Approximation (CA), where these are approximated by a constant value \mathcal{D} of the order of 10 MeV [28]. This greatly simplifies the numerical calculations, and it will be done here. Eq. (22) becomes

$$\begin{aligned} M_X^{0\nu^\mp}(0_f) &= \sum_J \sum_{p_1 p_2 n_1 n_2} \bar{\varrho}^\mp(p_1 n_1 p_2 n_2; J, 0_f) \\ &\times m_X^{0\nu}(p_1 n_1 p_2 n_2; J, \mathcal{D}), \end{aligned} \quad (23)$$

where the densities $\bar{\varrho}^\mp(p_1 n_1 p_2 n_2; J, 0_f)$ are given by (17).

The single particle $0\nu\beta\beta$ NMEs can be derived from [30, Eqs. (20)], and they are:

$$m_V^{0\nu}(p_1 p_2 n_1 n_2; J, \mathcal{D}) = W_{J0J}(p_1 n_1) W_{J0J}(p_2 n_2) \times \mathcal{R}_{JJ}^V(p_1 n_1 p_2 n_2; \mathcal{D}), \quad (24)$$

$$m_A^{0\nu}(p_1 p_2 n_1 n_2; J, \mathcal{D}) = \sum_L W_{L1J}(p_1 n_1) W_{L1J}(p_2 n_2) \times (-)^{L+1} \mathcal{R}_{LL}^A(p_1 n_1 p_2 n_2; \mathcal{D}), \quad (25)$$

$$m_P^{0\nu}(p_1 p_2 n_1 n_2; J, \mathcal{D}) = - \sum_{LL'l} (-)^{J+(L+L')/2} \hat{L} \hat{L}' (LL'l) \times (11|l) W_{L1J}(p_1 n_1) W_{L'1J}(p_2 n_2) \times \left\{ \begin{matrix} L & L' & l \\ 1 & 1 & J \end{matrix} \right\} \mathcal{R}_{LL'}^P(p_1 n_1 p_2 n_2; \mathcal{D}), \quad (26)$$

and

$$m_M^{0\nu}(p_1 p_2 n_1 n_2; J, \mathcal{D}) = - \sum_{LL'l} (-)^{J+(L+L')/2} \hat{L} \hat{L}' (LL'|l) \times (11|l) W_{L1J}(p_1 n_1) W_{L'1J}(p_2 n_2) \left[2 - \frac{l(l+1)}{2} \right] \times \left\{ \begin{matrix} L & L' & l \\ 1 & 1 & J \end{matrix} \right\} \mathcal{R}_{LL'}^M(p_1 n_1 p_2 n_2; \mathcal{D}). \quad (27)$$

We note that $m_V^{0\nu}$, and $m_A^{0\nu}$ are usually written as $m_F^{0\nu}$, and $m_{GT}^{0\nu}$, and that the $l = 2$ parts in $m_P^{0\nu}$, and $m_M^{0\nu}$ are the tensor components of $M^{0\nu}$.

The two-body radial integrals are defined as (see [26])

$$\mathcal{R}_{LL'}^X(p_1 n_1 p_2 n_2; \mathcal{D}) = r_N \int dk k^2 v_X(k; \mathcal{D}) \times R_L(p_1 n_1; k) R_{L'}(p_2 n_2; k), \quad (28)$$

with

$$R_L(pn; k) = \int_0^\infty u_{n_p l_p}(r) u_{n_n l_n}(r) j_L(kr) r^2 dr, \quad (29)$$

and

$$v_X(k; \mathcal{D}) = \frac{2}{\pi} \frac{\mathcal{G}_X(k)}{k(k+\mathcal{D})}, \quad (30)$$

where $\mathcal{G}_X(k) = g_V^2(k), g_A^2(k), k^2 f_M^2(k)$, and $k^2 g_P(k)[2g_A(k) - k^2 g'_P(k)]$, for $X = V, A, M$, and P , respectively. The ratio $r_N = 1.2A^{1/3}$ fm is introduced to make the $0\nu\beta\beta$ NMEs dimensionless [20].

The $\beta\beta$ -decay half-lives are evaluated from

$$[\tau(\mathcal{J}_f)]^{-1} = \mathcal{F}^2 |M(\mathcal{J}_f)|^2 G(\mathcal{J}_f), \quad (31)$$

where the $\beta\beta$ -decay mode factors are $\mathcal{F}_{2\nu} = 1$, and $\mathcal{F}_{0\nu} = \langle m_\nu \rangle$, with $\langle m_\nu \rangle$ given in natural units ($\hbar = m_e = c = 1$).

2.4 DCE Giant Resonances

In the present work, we will go a few steps further than what has been done in Refs. [14–17], comparing the NMEs in all final states that are reached by the $\beta\beta$ -decay, and not only in the ground state, and extending this study along the full strength distributions for the $0\nu\beta\beta$ -decays and DCE reactions, up to the region of DCE giant resonances. For this purpose, we introduce two new quantities:

1) The total $0\nu\beta\beta^\mp$ strengths $S^{0\nu^\mp}$, and their energy distributions $s^{0\nu^\mp}(0_f^+)$, define as

$$S^{0\nu^\mp} = \sum_f |M^{0\nu^\mp}(0_f^+)|^2 \equiv \sum_f s^{0\nu^\mp}(0_f^+), \quad (32)$$

as well as the ratios

$$R^{0\nu^\mp}(0_f^+) = s^{0\nu^\mp}(0_f^+)/S^{0\nu^\mp}; \quad (33)$$

and

2) The folded transition densities in $(A, Z \pm 2)$ nuclei

$$\mathcal{S}_{JJ}^{\{\mp 2\}}(\mathcal{E}) = \frac{\Delta}{\pi} \sum_f \frac{s_{JJ}^{\{\mp 2\}}(\mathcal{J}_f)}{(\mathcal{E} - \mathcal{E}_f)^2 + \Delta^2}, \quad (34)$$

as a function of excitation energies

$$\mathcal{E}_f = E_{0_f^+}^{\{\mp 2\}} - E_{0_1^+}^{\{\mp 2\}}, \quad (35)$$

of the final states $|0_f^+\rangle$, with the energy interval $\Delta = 1$ MeV.

The transitions $S_V^{0\nu^\mp}$, $S_{V_0}^{0\nu^\mp}$, $S_A^{0\nu^\mp}$, and $S_{A_{1+}}^{0\nu^\mp}$, and the rates $R_V^{0\nu^\mp}(0_f^+)$, $R_{V_0}^{0\nu^\mp}(0_f^+)$, $R_A^{0\nu^\mp}(0_f^+)$, and $R_{A_1}^{0\nu^\mp}(0_f^+)$, as well as the corresponding folded transition densities for $M_V^{0\nu^\mp}$, $M_A^{0\nu^\mp}$, $M_{V_0}^{0\nu^\mp}$ and $M_{A_1}^{0\nu^\mp}$, are defined in the same way.

The reaction folded strength densities meet the relationship

$$\int d\mathcal{E} \mathcal{S}_{J\mathcal{J}}^{\{\mp 2\}}(\mathcal{E}) = S_{J\mathcal{J}}^{\{\mp 2\}}, \quad (36)$$

and the same holds for $\mathcal{S}_V(\mathcal{E})$, and $\mathcal{S}_A(\mathcal{E})$.

Note that, due to the neutron excess, in the medium and heavy nuclei, it occurs that

$$S_{J\mathcal{J}}^{\{-2\}} \gg S_{J\mathcal{J}}^{\{+2\}}, \text{ and } S_{V,A}^{0\nu^-} \gg S_{V,A}^{0\nu^+}. \quad (37)$$

2.5 Q-Values

The Q -values for the $\beta\beta^-$ -decay, and for the ee -capture, are defined as

$$\begin{aligned} Q_{\beta\beta^-} &= \mathcal{M}(Z, A) - \mathcal{M}(Z + 2, A), \\ Q_{ee} &= \mathcal{M}(Z, A) - \mathcal{M}(Z - 2, A), \end{aligned} \quad (38)$$

where the \mathcal{M} 's are the atomic masses. When expressed by means of the energies $E_{0^+}^{\{0\}}$, and $E_{0^+}^{\{\pm 2\}}$ that have been defined above, they read

$$\begin{aligned} Q_{\beta\beta^-} &= E_{0^+}^{\{0\}} - E_{0^+}^{\{-2\}} \\ Q_{ee} &= E_{0^+}^{\{0\}} - E_{0^+}^{\{+2\}}. \end{aligned} \quad (39)$$

The above-mentioned observables are evaluated within different models of nuclear structure. Among them, the pn -QRPA is currently the most widely used nuclear model for estimating the NMEs for the $\beta\beta$ -decays to the ground state 0_1^+ ⁴. We have recently developed a new nuclear model for the DCE processes, based on the Quasiparticle Tamm-Dancoff Approximation (QTDA) for the pn and $2p2n$ excitations [36]. It is a natural extension of the original QRPA [38], and will be labeled DCEQTDA ⁵. The graphical representation of the two models is given in [36, Fig. 1]. The difference between them is cardinal, and has very important consequences, both analytical and numerical. Below, we present the corresponding formulation within the DCEQTDA.

⁴The SCE QRPA model was developed by Halbleib and Sorensen in 1967 [38] to describe the β -decay. Later, in the 1990s, averaging over two β -decays, this QRPA was adapted for $\beta\beta$ -decay calculations [22, 35, 39–46]. The unfavorable aspects of the pn -QRPA model are that: 1) It cannot describe $\beta\beta$ -decays to excited states, and 2) It does not allow the evaluation of the total strengths (2), and therefore neither the sum rules (5) nor the ratios $R_J^{\{\mp 2\}}(\mathcal{J}_f^+)$ given by (33), cannot be discussed either

⁵This model has been proposed, and applied in its particle-hole limit for $\beta\beta$ -decay in ^{48}Ca , long years ago [47].

3 DCEQTDA Nuclear Model

The basic assumption in the DCEQTDA is that the nuclei (A, Z) , $(A, Z \pm 1)$ and $(A, Z \pm 2)$ can be represented, respectively, as the BCS vacuum in the initial nucleus, and the excitations of two pn and four $2p2n$ quasiparticles in this vacuum. The resulting eigenvalue problem is discussed in detail in our previous work [36], where the model is labeled as $2p2n$ -QTDA.

In the present work, we only deal with the resulting wave functions

$$\begin{aligned} |J_i\rangle &= \sum_{pn} X_{pnJ_i} |pnJ\rangle, \\ |\mathcal{J}_f\rangle &= \sum_{p_1 p_2 n_1 n_2} \mathcal{X}_{p_1 p_2 J_p, n_1 n_2 J_n; \mathcal{J}_f} |p_1 p_2 J_p, n_1 n_2 J_n; \mathcal{J}\rangle, \end{aligned} \quad (40)$$

and the corresponding energies ω_{J_i} and $\Omega_{\mathcal{J}_f}$, for the intermediate and final nuclei, respectively. Here

$$\begin{aligned} |pnJ\rangle &\equiv A^\dagger(pnJ)|BCS\rangle, \\ |p_1 p_2 J_p, n_1 n_2 J_n; \mathcal{J}\rangle &\equiv [A^\dagger(p_1 p_2 J_p) A^\dagger(n_1 n_2 J_n)]_{\mathcal{J}} |BCS\rangle, \end{aligned} \quad (41)$$

are, respectively, the intermediate proton-neutron two quasiparticle states, and the final two protons two neutron states, being

$$A^\dagger(abJ) = N(ab)[a_a^\dagger a_b^\dagger]_J, \quad N(ab) = \frac{1}{\sqrt{1 + \delta_{ab}}}, \quad (42)$$

normalized two-quasiparticle states. and a_a^\dagger and the single-quasiparticle creation operators, defined by the Bogoljubov transformation [48, Eqs. (13.10)]. The BCS ground state is defined as $a_k |BCS\rangle = 0$.

The amplitudes X_{pnJ_i} , and $\mathcal{X}_{p_1 p_2 J_{12}, n_1 n_2 J'_{12}; \mathcal{J}_f^+}$, as well as the energies ω_{J_i} and $\Omega_{\mathcal{J}_f}$, are obtained by diagonalizing the Hamiltonian [49, 50]

$$H = H_0 + H_{pn} + H_{nn} + H_{pp}, \quad (43)$$

in both bases (41), *i.e.*, solving two different eigenvalue problems

$$\begin{aligned} H|J_i\rangle &\equiv (H_0 + H_{pn})|J_i\rangle = w_{J_i}|J_i\rangle, \\ H|\mathcal{J}_f^+\rangle &\equiv (H_0 + H_{pn} + H_{nn} + H_{pp})|\mathcal{J}_f^+\rangle = \Omega_{\mathcal{J}_f^+}|\mathcal{J}_f^+\rangle, \end{aligned} \quad (44)$$

the first for the intermediate nucleus, obtaining the amplitudes X_{pnJ_i} , and the second for the final nucleus, obtaining the amplitudes $\mathcal{X}_{p_1 p_2 J_{12}, n_1 n_2 J'_{12}; \mathcal{J}_f^+}$. Here $H_0 = \sum_a E_a a_a^\dagger a_a$ is the independent-quasiparticle Hamiltonian, and H_{nn} , H_{pp} , and H_{pn} are, respectively, neutron-neutron, proton-proton, and proton-neutron residual interactions among quasiparticles. Obviously, H_{nn} , and H_{pp} are not involved in the first of these two equations, since in (44)

$H_{nn}|pnJ_i\rangle = H_{pp}|pnJ_i\rangle = 0$. Details on the evaluation of matrix elements of H can be found in References [49, 50].

As discussed in Ref. [30], in the pn -QRPA calculation of the $\beta\beta$ -decay is based on the next approximations:

i) In (14),

$$\langle \mathcal{J}_f^+ | | \mathcal{O}_J^\pm | | J_i^+ \rangle \cong \langle \bar{J}_i^+ | | \mathcal{O}_J^\mp | | \bar{0}^+ \rangle = \sum_{pn} \rho^\mp(pn, \bar{J}_i^\pi) W_{J_0 J}(pn),$$

where $|\bar{0}^+\rangle$ and $|\bar{J}_i^+\rangle$ are, respectively, the ground states in the final nucleus, and the pn excitations on it, and

ii) In (19),

$$E_{0^+}^{\{0\}} - E_{0_1^+}^{\{-2\}} \cong Q_{\beta\beta^-}, \quad E_{0^+}^{\{0\}} - E_{0_1^+}^{\{+2\}} \cong Q_{ee},$$

being $Q_{\beta\beta^-}$, and Q_{ee} taken from the experimental data for the Q -values (see (39)).

That is, one needs to compute the one-body F/GT transition matrix elements starting from both initial and final nuclei, and then match the intermediate states by computing the overlaps of their wave functions [51].

As a consequence, in the standard pn -QRPA [40] calculations, in addition to solving the BCS equation for the initial nucleus (A, Z), and working with the initial occupation coefficients (v_p, v_n)⁶, as we do in DCEQTDA, we must also solve the BCS equation for the final nucleus ($A, Z + 2$), or ($A, Z - 2$), and also deal with the final occupation coefficients (\bar{v}_p, \bar{v}_n). Moreover, in the non-standard pn -QRPA only one BCS equation is solved, but for intermediate nucleus ($A, Z + 1$), or ($A, Z - 1$) (See Ref. [30], and references therein).

In the DCEQTDA, the wave functions of the final nucleus $|\mathcal{J}_f\rangle$ are constructed directly on top of the wave function of the initial nucleus in terms of the $2p2n$ quasiparticle excitations. These wave functions, which do not exist in the pn -QRPA, are then used to evaluate the two-body NMEs of $\beta\beta$ -decay.

The β^- -decay densities are evaluated from Eq. (3) and Eq. (4), with the results

$$\varrho^-(p_1 n_1; J_i) = \sum_{pn J_p} u_{p_1} v_{n_1} X_{p_1 n_1 J_i}, \quad (45)$$

and

$$\begin{aligned} \varrho^-(p_2 n_2; J_i, \mathcal{J}_f^+) &= \hat{J} \hat{\mathcal{J}}_f \sum_{pn J_p J_n} (-)^{J_p + J_n} \hat{J}_p \hat{J}_n \\ &\times N(nm_2) N(pp_2) \mathcal{X}_{pp_2 J_p, nn_2 J_n; \mathcal{J}_f} \end{aligned}$$

⁶The u 's and v 's in the initial nucleus are determined under the constraints $\sum_{j_p} (2j_p + 1) v_p^2 = Z$, and $\sum_{j_n} (2j_n + 1) v_n^2 = N$, where Z and N are the number of protons and neutrons, respectively, in the initial nucleus.

$$\times \bar{P}(nn_2J_n)\bar{P}(pp_2J_p) \begin{Bmatrix} p & p_2 & J_p \\ n & n_2 & J_n \\ J & J & \mathcal{J} \end{Bmatrix} u_{p_2}v_{n_2}X_{pnJ_i}, \quad (46)$$

where $\hat{J} = \sqrt{2J+1}$, and

$$N(ab) = (1 + \delta_{ab})^{-1/2}, \quad (47)$$

is the two particle normalization factor. The operator

$$\bar{P}(p_1p_2J) = 1 - (-)^{p_1+p_2-J}P(p_1 \leftrightarrow p_2), \quad (48)$$

takes into account the Pauli Exclusion Principle by exchanging among valence quasiparticles p_1 and p_2 , and acts only on the right hand side [50].⁷

The corresponding β^+ -decay densities density matrices $\varrho^+(p_1n_1; J_i)$, and $\varrho^+(p_2n_2; J_i, \mathcal{J}_f^+)$ are obtained from Eq. (49) and Eq. (50), respectively, after making $u_{p_1}v_{n_1} \rightarrow u_{n_1}v_{p_1}$, and $u_{p_2}v_{n_2} \rightarrow u_{n_2}v_{p_2}$.

The two-body density matrix $\varrho^-(p_1n_1p_2n_2; J_i, \mathcal{J}_f)$, and $\bar{\varrho}^-(p_1n_1p_2n_2; J\mathcal{J}_f)$ evaluated, respectively, from Eqs. (15) and (17) are

$$\begin{aligned} & \varrho^-(p_1n_1p_2n_2; J_i\mathcal{J}_f^+) = \hat{J}\hat{\mathcal{J}}_f \\ & \times \sum_{pnJ_pJ_n} (-)^{J_p+J_n} \hat{J}_p\hat{J}_n N(nn_2)N(pp_2) \\ & \times \mathcal{X}_{pp_2J_p, nn_2J_n; \mathcal{J}_f} \bar{P}(nn_2J_n)\bar{P}(pp_2J_p) \\ & \times \begin{Bmatrix} p & p_2 & J_p \\ n & n_2 & J_n \\ J & J & \mathcal{J} \end{Bmatrix} u_{p_2}v_{n_2}X_{pnJ_i}u_{p_1}v_{n_1}X_{p_1n_1J_i}, \end{aligned} \quad (49)$$

and

$$\begin{aligned} & \bar{\varrho}^-(p_1n_1p_2n_2; J\mathcal{J}_f) = \hat{J}\hat{\mathcal{J}}_f \\ & \times \sum_{J_pJ_n} (-)^{J_p+J_n} \hat{J}_p\hat{J}_n N(n_1n_2)N(p_1p_2) \\ & \times \mathcal{X}_{p_1p_2J_p, n_1n_2J_n; \mathcal{J}_f} \bar{P}(n_1n_2J_n)\bar{P}(p_1p_2J_p) \end{aligned}$$

7

$$\begin{aligned} & \varrho^-(p_2n_2; J_i, 0_1^+) \\ & = \sum_{pnJ_p} \hat{J}_p N(nn_2)N(pp_2)\mathcal{X}_{pp_2J_p, nn_2J_p; 0_1} \\ & \times \bar{P}(nn_2J_p)\bar{P}(pp_2J_p) \\ & \times (-)^{p_2+n_2+J_p+J} \begin{Bmatrix} p & p_2 & J_p \\ n_2 & n & J \end{Bmatrix} u_{p_2}v_{n_2}X_{pnJ_i}, \end{aligned}$$

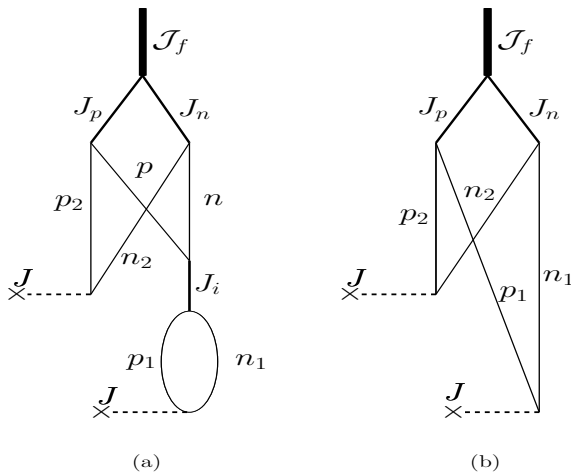


Fig. 1 Two-body transition densities $\varrho(p_1 n_1 p_2 n_2; J_i \mathcal{J}_f)$, given by (49), and used in the evaluation of $M^{2\nu}(\mathcal{J}_f)$, and $\bar{\varrho}(p_1 n_1 p_2 n_2; J J_f)$, given by (50), and used to calculate $M^{0\nu}(0_f^+)$ within the CA and to $M_J(\mathcal{J}_f)$, are shown in panels (a) and (b), respectively. The dashed lines indicate the single β -decays. The first β -decay is activated in the initial state, and the second in the intermediate state. The five vertices of these diagrams correspond to five of the six angular momentum couplings in the symbol $9j$ in Eqs. (49) and (50). The sixth coupling $(JJ)\mathcal{J}$ corresponds to the three unconnected lines.

$$\times \left\{ \begin{array}{ccc} p_1 & p_2 & J_p \\ n_1 & n_2 & J_n \\ J & J & \mathcal{J} \end{array} \right\} u_{p_2} v_{n_2} u_{p_1} v_{n_1}. \quad (50)$$

The graphical representations of densities $\varrho(p_1 n_1 p_2 n_2; J_i^\pi \mathcal{J}_f^+)$, and $\bar{\varrho}(p_1 n_1 p_2 n_2; J^\pi \mathcal{J}_f^+)$ are exhibited, respectively, in panels (a), and (b) of Fig. 1.

The energies of the intermediate state $|J_i\rangle$ and the final state $|\mathcal{J}_f\rangle$, relative to the initial state $|0^+\rangle$, are [36, 52, 53]

$$\begin{aligned} E_{J_i}^{\{\mp 1\}} - E_{0^+}^{\{0\}} &= \omega_{J_i} \pm \lambda_p \mp \lambda_n, \\ E_{\mathcal{J}_f}^{\{\mp 2\}} - E_{0^+}^{\{0\}} &= \Omega_{\mathcal{J}_f} \pm 2\lambda_p \mp 2\lambda_n, \end{aligned} \quad (51)$$

where λ_p and λ_n are the proton and neutron chemical potentials, which are omitted in many pn -QRPA calculations, But, the energy denominator (19), which becomes

$$\mathcal{D}_{J_i, \mathcal{J}_f} = \omega_{J_i} - \frac{\Omega_{\mathcal{J}_f}}{2}, \quad (52)$$

being the same for $\beta\beta^\mp$ -decays, does not depend of them.

Contrarily, the Q -values, for the $\beta\beta^-$ -decay and for the ee -capture, in the present model, are given by

$$\begin{aligned} Q_{\beta\beta^-} &= -\Omega_{0_1^+} - 2(\lambda_p - \lambda_n), \\ Q_{ee} &= -\Omega_{0_1^+} + 2(\lambda_p - \lambda_n). \end{aligned} \quad (53)$$

These are the windows of excitation energies where $\beta\beta$ -decay and the ee -capture can be observed. Note that their difference

$$\Delta Q \equiv Q_{ee} - Q_{\beta\beta^-} = 4(\lambda_p - \lambda_n), \quad (54)$$

depends solely on the mean field, i.e. on the difference between the chemical potentials.⁸

4 Numerical Results and Discussion

As mentioned above, the main objective of this work is the evaluation of the $0\nu\beta\beta$ NMEs, within the DCEQTDA model, both analytically and numerically. The latter is done in Section 4.3 by making use of Eqs. (22), (24)-(27), and (53). Previously, in Section 4.1 we explain how the numerical calculations are performed within this new model, and in Section 4.2 we show the results for the DCE observables measured so far in ^{76}Ge and ^{124}Xe . This is for: the DCE Q -values $Q_{\beta\beta^-}$, and Q_{ee} , and for the excitation energies $\mathcal{E}_{\mathcal{J}_f^+}$ in the final nuclei, using, respectively, Eqs. (39), and (51), and for (ii) the NMEs $M_{\mathcal{J}_f^+}^{2\nu^\mp}(\mathcal{J}_f)$, employing (16), and (18). We proceed similarly with the remaining nuclei.

4.1 Residual Interaction and Single Particle Energies

We describe the residual interaction in (43), i.e in H_{pn} , H_{nn} , and H_{pp} with the same δ -force

$$V = -4\pi(v^s P_s + v^t P_t)\delta(r) \quad \text{MeV}\cdot\text{fm}^3, \quad (55)$$

because of its simplicity, and because in this way a comparison can be made between the present DCEQTDA, and our previous pn -QRPA calculations of the 0ν NMEs [Fig. 3][30].

To highlight the differences between the two models, we will use here the same parameterization that was used in the pn -QRPA:

1) The pairing strengths for protons and neutrons, $v_{\text{pair}}^s(p)$ and $v_{\text{pair}}^s(n)$ were obtained from the fitting of the corresponding experimental pairing gaps.

2) The isovector (v^s) and isoscalar (v^t) parameters within the particle-particle (pp) and particle-hole (ph) channels, as well as the ratios $s = v_{\text{pp}}^s/\bar{v}_{\text{pair}}^s$,

⁸It might be interesting to note that the chemical potentials λ_p , and λ_n in Eqs. (51), are the same as in [36, Eq.(2.38)], [52, page 58], and [53, pages 235-237]. Moreover, while they play no role in the pn -QRPA, in the DCEQTDA they allow us to evaluate the Q -values (53), which agree with the experimental data, as seen in [36, [Table Vi], and here in Table I.

and $t = v_{pp}^t/\bar{v}_{pair}^s$, with $\bar{v}_{pair}^s = (v_{pair}^s(p) + v_{pair}^s(n))/2$, were fixed in the same way as in our QRPA calculations [30, 36] (see [30, Fig. 1]). That is, they are determined from the condition that the strengths $S_J^{\{+1\}}$ become minimal, with the result $s = s_{sym} = 1$, and $t = t_{sym} \gtrsim 1$, and which is named Partial SU(4) Symmetry Restoration (PSU4SR).

In the present case we have $t_{sym} = 1.34$ for ^{76}Ge , and $t_{sym} = 1.42$ for ^{124}Xe . This parametrization will be labeled as P1. We have found it convenient to show in the case of ^{76}Ge also the results for the value of the parameter t that reproduces the measured value of the ground state 2ν NME. This is frequently done in the literature [28], with the result here $t = 1.86$, which we will label as P2.

All NMEs were evaluated with the measured value $g_A = 1.27$ [31]. The $\beta\beta$ -decay half-lives were calculated from (31), and all kinematics factors $G_{2\nu}(\mathcal{J}_f^+)$, and $G_{0\nu}(\mathcal{J}_f^+)$ were taken from [54], except for $G_{2\nu}(2_2^+)$ in ^{76}Ge that was found in [55].

Although the most recent pn-QRPA calculations [37] include many single-particle levels (18 for ^{76}Ge , and 26 for ^{130}Xe), we choose single-particle spaces such that they satisfy the sum rules (10) and (11), for which they must have a sufficiently large number of states, these being the same for protons and neutrons, and always including the two spin-orbit partners. At the same time, they must be numerically tractable in DCEQTDA. The single-particle energies were obtained from the Wood-Saxon potential with the standard parameterization [56].

Thus, we use 9 single-particle levels ($2d_{3/2}$, $1g_{7/2}$, $3s_{1/2}$, $2d_{5/2}$, $1g_{9/2}$, $2p_{1/2}$, $1f_{5/2}$, $2p_{3/2}$, and $1f_{7/2}$) in ^{76}Ge , and 7 levels ($1h_{7/2}$, $1h_{9/2}$, $2d_{3/2}$, $1g_{7/2}$, $3s_{1/2}$, $2d_{5/2}$, and $1g_{9/2}$) in ^{124}Xe . The number of resulting four quasiparticle states $|\mathcal{J}^+\rangle$, defined in Eq. (40), are 2045 states $|0^+\rangle$, and 8456 states $|2^+\rangle$ in ^{76}Se , and 1146 states $|0^+\rangle$, and 4918 states $|2^+\rangle$ in ^{124}Te . Some calculations have been performed on this nucleus with 9 levels, including also the states $1f_{7/2}$ and $1f_{5/2}$. The number of resulting four quasiparticle states $|\mathcal{J}^+\rangle$, define in Eq. (40), are 2045 states $|0^+\rangle$, and 8456 states $|2^+\rangle$ in ^{76}Se , and 1146 states $|0^+\rangle$, and 4918 states $|2^+\rangle$ in ^{124}Te .

4.2 Measured DCE Observables

First, we will focus on the DCE observables that have been experimentally measured, and will serve to test the nuclear model used. This will be done for the $\beta\beta$ -decay in ^{76}Ge , and for the ee -capture in ^{124}Xe , analyzing:

a) The Q -values, defined in (39), that were evaluated from (53), and are given in Table 1. The agreement between the data and the calculations is quite reasonable. It should be noted that we obtain that $Q_{\beta\beta^-}$ is positive and Q_{ee} negative for ^{76}Ge , and opposite for ^{124}Xe , which, although expected, is not a trivial result.

b) The excitation energies $\mathcal{E}_{\mathcal{J}_f^+}$ in the final nucleus, defined by (51), and the 2ν NMEs for $\mathcal{J}_f^+ = 0_{1,2}^+$, and $2_{1,2}^+$, both are listed in Table 2. All energies

Table 1 Calculated and experimental Q -values (in MeV) for ^{76}Ge . The parameterizations P1, and P2 are explained in the text.

Par/Exp	$Q_{\beta\beta^-}$	Q_{ee}	ΔQ
^{76}Ge			
P1	1.239	-8.240	-9.479
P2	1.314	-8.164	-9.478
Exp. [57]	2.039	-10.910	-12.95
^{124}Xe			
P1	-9.403	4.071	13.474
Exp. [57]	-8.572	2.864	11.436

are reasonably well reproduced, except $\mathcal{E}_{2_1^+}$ in ^{124}Te , which turned out to be negative.

The DCEQTDA prediction of 2^+ state as ground state in ^{124}Te is obviously incorrect, since in nature the ground state in even-even nuclei is always the 0^+ state. In theoretical calculations this only necessarily occurs in the case of having two identical particles, for which there is only one state for each total angular momentum, and when they interact with each other with the pure pairing force. Here we work with the δ -force (55), where the pairing interaction is dominant, but other multipoles are also involved. Moreover, as already mentioned, in the case of ^{124}Te , we deal with 4 non-identical particles, where there are 1146 $|0^+\rangle$ states, and 4918 $|2^+\rangle$ states, which makes a big difference. The collective (vibrational) degrees of freedom play an important role in the even isotopes of Te, and must be taken into account in any realistic calculation. (See, for example, Ref. [58]).

c) The corresponding half-lives $\tau_{2\nu}$ are also shown, and compared with the experimental data [6, 18, 59]. All our computed half-lives $\tau_{2\nu}(\mathcal{J}_f^+)$ are consistent with the measurements.

For comparison, Table 2 further shows the calculations in ^{76}Ge performed within: i) the Multiple-Commutator Model (MCM) [60]⁹, the Shell Model (SM) [61], as well as the calculations in ^{124}Xe performed within: i) MCM [60], and ii) the Effective Theory (ET), and the SM [62].

The fact that the agreement with experiments is satisfactory for the nuclei ^{76}Ge and ^{124}Xe , as well as for ^{48}Ca , and ^{86}Ru , which we have previously performed in Ref. [36], suggests the reliability of the nuclear structure model DCEQTDA. Despite this, the question remains pertinent as to whether the inclusion of other nuclei would change the conclusions about its validity. The answer is the opposite, and that the more analysed cases, the more the validity of the DCEQTDA model is confirmed, as shown in Table 7, which is delegated to the Appendix so that reading the article does not become too tedious, due to the large amount of material it includes.

⁹The MCM is in fact a superposition of two different nuclear models, each with its own parameterisation. One is the charge-exchange pn-QRPA, used to describe the intermediate states $|J_i\rangle$, and the other is a charge-conserving QRPA, used to describe the excited final states $|J_f^+\rangle$.

Table 2 Calculated and experimental excitation energies $\mathcal{E}_{J_f^+}$ in ^{76}Se , the NMEs $M^{2\nu}(J_f^+)$, and half-lives $\tau_{2\nu}(J_f^+)$ for the decays of ^{76}Ge , and ^{124}Xe to $J_f^+ = 0_{1,2}^+$, and $2_{1,2}^+$ states in ^{76}Se , and ^{124}Te , respectively, with parameterizations P1 and P2, and with $g_A = 1.27$ [31]. This table also shows the calculations in ^{76}Ge performed within: i) the Multiple-Commutator Model (MCM), [51], and ii) the Shell Model (SM) [61], as well as the calculations in ^{124}Xe performed within: i) MCM [60], and ii) the Effective Theory (ET), and the SM [62], where all NMEs are multiplied by $(g_A = 1.27)^2$. The experimental ground state $\tau_{2\nu}^{ee}(J_f^+)$ is from Ref. [18]. The measured half-lives in ^{76}Se are from [59] for the ground state, and from [7] for the excited states, and the experimental $\tau_{2\nu}^{ee}$ in ^{124}Te is from Ref. [18]. All G factors are from Ref. [54], except that of the 2_2^+ state in ^{76}Se , which is from Ref. [55].

$^{76}\text{Ge} \rightarrow ^{76}\text{Se}$	J_f^+	0_1^+	0_2^+	2_1^+	2_2^+
\mathcal{E} (MeV)					
	P1	0.0	2.13	0.36	1.98
	P2	0.0	2.13	0.26	1.90
	Exp.	0.0	1.12	0.56	1.22
$ M^{2\nu} $ (n.u.)		$\times 10^3$	$\times 10^3$	$\times 10^3$	$\times 10^3$
	P1	56.4	80.1	2.8	5.2
	P2	103	158	6.6	12.3
	SM	97	70	0.7	1.8
	MCM	74	363	1	3
	Exp.	107	< 147	< 58	< 873
$\tau_{2\nu}$ (yr)		$\times 10^{21}$	$\times 10^{23}$	$\times 10^{23}$	$\times 10^{24}$
	P1	6.8	25	$3.3 \cdot 10^3$	$3.6 \cdot 10^4$
	P2	2.0	6.5	$6.0 \cdot 10^2$	$6.5 \cdot 10^3$
	Exp.	1.88	> 7.5	> 7.7	> 1.3
$^{124}\text{Xe} \rightarrow ^{124}\text{Te}$	J_f^+	0_1^+	0_2^+	2_1^+	2_2^+
\mathcal{E} (MeV)					
	P1	0.0	1.74	-0.16	1.62
	Exp.	0.0	1.66	0.60	1.32
$ M^{2\nu} $ (n.u.)		$\times 10^3$	$\times 10^3$	$\times 10^3$	$\times 10^3$
	P1	62	46	7.1	8.3
	ET	18 – 66	3.2 – 80	0.13 – 1.45	
	SM	45 – 116	8 – 16	0.17 – 0.37	
	MCM	476	15	1.1	
	Exp.	57 ± 10			0.11
$\tau_{2\nu}$ (yr)		$\times 10^{22}$	$\times 10^{25}$	$\times 10^{28}$	
	P1	1.51	0.28	0.14	
	ET	18.6 – 1.33	57.8 – 0.92	435 – 3.45	
	SM	2.87 – 0.43	9.21 – 2.34	231 – 52.6	
	MCM	0.026	2.66	5.99	
	Exp.	1.8 ± 0.5			

Table 3 Fine structure of $M^{0\nu}(0_1^+)$ for ^{76}Ce , evaluated in the pn -QRPA and DCEQTDA with the same parametrization P1 in both cases. The contributions of different intermediate-state angular momenta J^π are listed for both parities $\pi = \pm$. The most relevant numbers are shown in bold type.

J^π	pn -QRPA						DCEQTDA								
	$M_V^{0\nu}$	$M_A^{0\nu}$	$M_M^{0\nu}$	$M_P^{0\nu}$	$M^{0\nu}$	$M_V^{0\nu}$	$M_A^{0\nu}$	$M_M^{0\nu}$	$M_P^{0\nu}$	$M^{0\nu}$	$M_V^{0\nu}$	$M_A^{0\nu}$	$M_M^{0\nu}$	$M_P^{0\nu}$	$M^{0\nu}$
0^+	0.020	0.000	0.000	0.000	0.020	0.145	0.000	0.000	0.000	0.145	0.000	0.000	0.000	0.000	0.145
1^+	0.000	-0.682	0.007	-0.022	-0.697	0.000	0.466	0.006	-0.027	0.445	0.000	0.466	0.006	-0.027	0.445
2^+	0.173	0.255	0.026	0.000	0.453	0.035	0.047	0.005	0.000	0.087	0.035	0.047	0.005	0.000	0.087
3^+	0.000	0.475	0.028	-0.172	0.330	0.000	0.077	0.004	-0.018	0.064	0.000	0.077	0.004	-0.018	0.064
4^+	0.080	0.121	0.022	0.000	0.223	0.011	0.014	0.003	0.000	0.027	0.011	0.014	0.003	0.000	0.027
5^+	0.000	0.230	0.024	-0.104	0.150	0.000	0.026	0.003	-0.008	0.021	0.000	0.026	0.003	-0.008	0.021
6^+	0.030	0.049	0.015	0.000	0.093	0.003	0.004	0.001	-0.000	0.008	0.003	0.004	0.001	-0.000	0.008
7^+	0.000	0.097	0.014	-0.045	0.066	0.000	0.009	0.001	-0.003	0.007	0.000	0.009	0.001	-0.003	0.007
8^+	0.009	0.014	0.005	0.000	0.028	0.001	0.001	0.000	0.000	0.002	0.001	0.001	0.000	0.000	0.002
9^+	0.000	0.056	0.012	-0.026	0.042	0.000	0.006	0.001	-0.002	0.005	0.000	0.006	0.001	-0.002	0.005
$\pi = +$	0.311	0.613	0.153	-0.368	0.708	0.194	0.650	0.024	-0.057	0.811	0.194	0.650	0.024	-0.057	0.811
0^-	0.000	0.054	0.000	-0.029	0.025	0.000	0.009	0.000	-0.003	0.006	0.000	0.009	0.000	-0.003	0.006
1^-	0.149	0.227	0.013	0.000	0.389	0.019	0.023	0.001	0.000	0.043	0.019	0.023	0.001	0.000	0.043
2^-	0.000	0.741	0.025	-0.170	0.596	0.000	0.148	0.004	-0.017	0.135	0.000	0.148	0.004	-0.017	0.135
3^-	0.107	0.230	0.031	0.000	0.368	0.011	0.028	0.004	0.000	0.043	0.011	0.028	0.004	0.000	0.043
4^-	0.000	0.398	0.033	-0.144	0.286	0.000	0.048	0.004	-0.009	0.043	0.000	0.048	0.004	-0.009	0.043
5^-	0.060	0.132	0.031	0.000	0.223	0.006	0.015	0.003	-0.000	0.024	0.006	0.015	0.003	-0.000	0.024
6^-	0.000	0.201	0.027	-0.084	0.144	0.000	0.018	0.002	-0.004	0.016	0.000	0.018	0.002	-0.004	0.016
7^-	0.028	0.064	0.023	0.000	0.115	0.003	0.006	0.002	0.000	0.012	0.003	0.006	0.002	0.000	0.012
8^-	0.000	0.050	0.010	-0.023	0.037	0.000	0.002	0.000	-0.000	0.002	0.000	0.002	0.000	-0.000	0.002
$\pi = -$	0.343	2.098	0.193	-0.451	2.183	0.039	0.296	0.021	-0.034	0.323	0.039	0.296	0.021	-0.034	0.323
Total	0.654	2.711	0.346	-0.819	2.891	0.234	0.946	0.045	-0.091	1.133	0.234	0.946	0.045	-0.091	1.133

4.3 $0\nu\beta\beta$ NMEs

4.3.1 Anatomy of $0\nu\beta\beta$ NMEs

In Table 3 we show the contributions of different intermediate states J^π to $M^{0\nu^-}(0_1^+)$ in ^{76}Se (positive parities in the top panel and negative parities in the bottom panel, evaluated in the pn -QRPA and DCEQTDA, with the same residual interaction (55) and the parametrization P1, and using the same set of single-particle energies in both cases.¹⁰

The most relevant partial NMEs in both nuclear models are shown in bold type, and are labelled as:

i) $M_{V_{0+}}^{0\nu}$, which is the contribution of intermediate states $J^\pi = 0^+$ to $M_{V}^{0\nu}$, and

ii) $M_{A_{1+}}^{0\nu}$, which is the contribution of intermediate states $J^\pi = 1^+$ to $M_A^{0\nu}$. It is important to note that the $0\nu\beta\beta$ NMEs differ from the $2\nu\beta\beta$ and reaction NMEs, not only in radial dependence but also in genesis. Indeed, while the first receive contributions from all intermediate states $J^\pi = 0^\pm, 1^\pm, \dots, 9^\pm$, the latter are constructed only from the intermediate states $J^\pi = 0^+(M_{V}^{2\nu}$, and $M_{00})$, and $J^\pi = 1^+(M_A^{2\nu}$, and $M_{10})$.

Table 3 also shows that:

i) In both nuclear models the Fermi (F), weak magnetism (M) and pseudoscalar (P) NMEs are small compared to the axial vector (A) ones.

ii) As a consequence, in both nuclear models the contributions of the intermediate states with $J^\pi = 1^+$ dominate those with $J^\pi \neq 1^+$, and, in particular, in the pn -QRPA are negative, and therefore interfere destructively¹¹. Despite this, the final result is that the total NME $M^{0\nu}$ in the DCEQTDA is significantly lower than that obtained in the pn -QRPA calculation.

There are several previous QRPA calculations on the anatomy of NMEs as a function of intermediate states [63–68], which were obtained using different single-particle spaces, and various residual interactions. They all lead to results that differ from each other, making it difficult to choose one to compare with ours. In this scenario, we will compare with those reported in the Ref. [67], done with two- nucleon interactions based on the Bonn one-boson-exchange G matrix. A similar study based on the shell model also exists [69], which will also be used in our discussion.

To facilitate the comparison of the last two mentioned works with ours, in Fig. 2 we show the total contributions of each intermediate state J^π to $M^{0\nu^-}(0_1^+)$ in ^{76}Se (positive parities in the upper panel and negative parity in the lower panel), which are listed in column 6 (for pn -QRPA) and in column 11 (for DCEQTDA) of Table 3. The same figure also shows the results obtained by Hyvärinen and Suhonen [67, Fig. 1]. From this comparison, we see that:

¹⁰With the P2 parameterization, similar results are obtained in the DCEQTDA, but the pn -QRPA in this case collapses.

¹¹Negative value of the 1^+ contribution ave been seen in ^{96}Zr , ^{100}Mo , and ^{124}Sn nuclei[64, 67]. The interference with the rest of the contributions reduces the magnitude of the final NME for these decays.

a) Except for the aforementioned sign of the intermediate $J^\pi = 1^+$ states, our pn -QRPA results agree qualitatively with the calculations performed in Ref. [67], using the same nuclear model. However, their value $M^{0\nu} = 5.26$ for the total NME is significantly larger than our result $M^{0\nu} = 2.89$, which is probably due to the use of a more realistic nucleon-nucleon interaction than the one we use.

b) On the other hand, our DCEQTDA calculations are consistent with the results obtained by Sen'kov and Horoi [69] in the SM. In fact, in both cases, the most important contributions to $M^{0\nu}$ come from intermediate states $J^\pi = 1^+$, and $J^\pi = 2^-$. These are, respectively 30%, and 15% in Ref. [69], and 39%, and 12% in our case (see Table 3). The difference in the total value of $M^{0\nu}$ (theirs = 3.374, and ours = 1.133) may come from the difference in both the residual interaction and the nuclear structure model used in the two calculations.

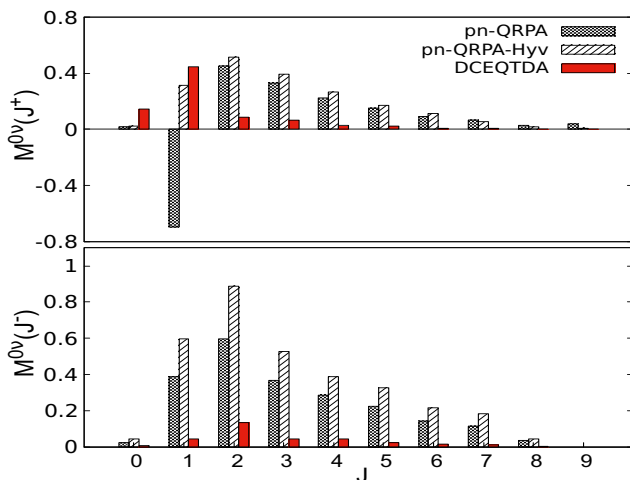


Fig. 2 Contributions of different intermediate-state angular momenta J^π to $M^{0\nu}(0_1^+)$ in ^{76}Se within present pn -QRPA, and DCEQTDA calculations, employing the same parametrization P2, and the pn -QRPA calculation done by Hyvärinen, and Suhonen [67]. Positive parities are shown in the upper panel and negative parities in the lower one.

4.3.2 Comparison of our results for 0ν NMEs with other calculations

In Fig. 3 we compare our pn -QRPA and DCEQTDA calculations for the ground-state $0\nu\beta\beta$, and $0\nu ee$ NMEs, performed with the same residual interaction and identical nuclear model parameters. We also show the results of pn -QRPA calculations done with more realistic residual interactions, such as the Argonne V18 or CD-Bonn potentials [66, 67], as well as the results of calculations with other nuclear models.

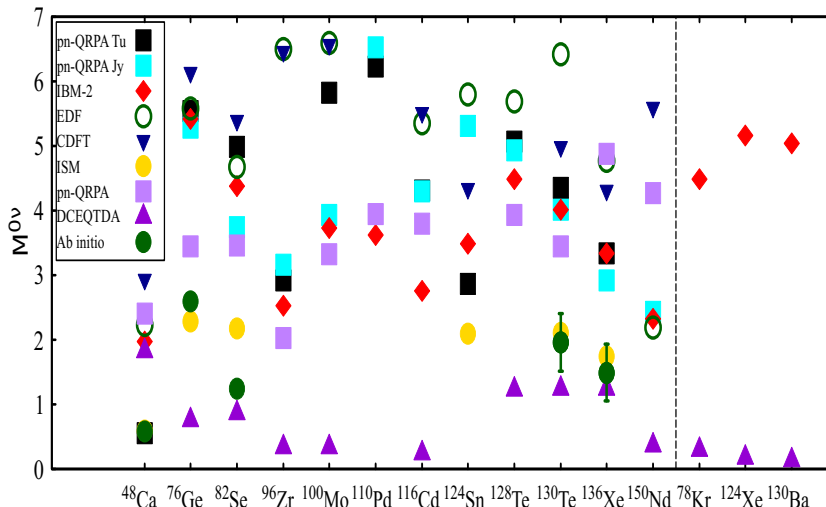


Fig. 3 (Color online) Comparison of calculated NMEs $M^{0\nu^-}(0_1^+) \equiv M^{0\nu}$, within several nuclear structure models: i) pn -QRPA by Tübingen group (QRPA Tu) [66] ($g_A = 1.27$), ii) pn -QRPA by Jyväskylä group (QRPA Jy) [67] ($g_A = 1.26$), iii) Interacting Boson Model (IBM-2) [74] ($g_A = 1.269$), iv) Energy Density Functional Method (EDF) [75] ($g_A = 1.25$), v) Covariant Density Functional Theory (CDFT) [34, 76] ($g_A = 1.254$), vi) Interacting Shell Model (ISM) [77] ($g_A = 1.25$), vii) The Ab initio Calculations in ^{48}Ca , ^{76}Ge , and ^{82}Se [70], in ^{130}Te [71], and in ^{136}Xe [72] viii) The present pn -QRPA and DCEQTDA results ($g_A = 1.27$).

It can be deduced that, except for ^{48}Ca , the new DCEQTDA model produces results that are definitely smaller than the other nuclear structure models; going from 0.12 in ^{116}Cd to 1.7 in ^{48}Ca for $0\nu\beta\beta$ NMEs, and from 0.14 in ^{130}Ba to 0.33 in ^{78}K for $0\nu ee$ NMEs. *Ab-initio* calculations of $0\nu\beta\beta$ NMEs, [70–72] are going in the same direction, but we have no idea what the reason for this is!

The fact that in the DCEQTDA model says the NMEs are much more smaller in the $0\nu ee$ -capture than in the $0\nu\beta\beta^-$ -decay, is fully consistent with Eq. (37), but strongly disagrees with the pn -QRPA and IBM calculations, shown in [73, Table III]. The relations (37) are completely independent of the nuclear model used and depend only on the neutron excess. However, in making the above comparison it should be noted that, as Fig. 4 indicates, most of the transition strengths $S_{V,A}^{0\nu^-}$ are concentrated in the region of giant resonances, far from the fundamental state of the final nucleus, and that such collective states do not appear in the strengths $S_{V,A}^{0\nu^+}$.

A more complete analysis of the $2\nu\beta\beta$ NMEs is given in Table 7, where the results for several nuclei are shown, in which double beta decay, and double electron capture processes take place.

4.3.3 Relation between $0\nu\beta\beta$, and Double Fermi and Double Gamow-Teller NMEs, within the DCEQTDA

The upper part of Table 4 presents the comparison between the calculations for: i) The $0\nu\beta\beta$ NMEs $M_V^{0\nu}$, $M_{V_{0^+}}^{0\nu}$, $M_A^{0\nu}$, $M_{A_{1^+}}^{0\nu}$, $M_P^{0\nu}$, $M_M^{0\nu}$, and $M^{0\nu}$, and ii) The absolute values of M_{00} , and M_{10} , for $\mathcal{J}_f^+ = 0_{1,2}^+$ states in ^{76}Se , with the P1 and P2 parameterizations.

From the discussion presented above in Section 4.3.1, it is easy to be convinced that physically M_{00} corresponds to $M_{V_{0^+}}^{0\nu}$, since both are generated only from intermediate states $J = 0^+$. The same is true for M_{10} and $M_{A_{1^+}}^{0\nu}$, which are generated only from intermediate states $J = 1^+$. Therefore it is not correct to associate M_{00} with $M_V^{0\nu}$, nor M_{10} with $M_A^{0\nu}$, as is often done. In previous comparisons between M_{10} and $M^{0\nu}$ [14–17], the results obtained for them in different calculations, and with different nuclear models were used.

The fact that $0\nu\beta\beta$ and DCER (Double Charge Exchange Reaction) NMEs turn out to be of the same order of magnitude is a surprise in view of the large differences between them (radial and energy dependencies, finite nucleon size effects, and short-range correlations taken into account in the former, etc). It should also be remembered that the nuclear radius r_N was introduced into $M^{0\nu}$ by Doi [20] some time ago in a rather arbitrary way, just to make it dimensionless (see (28)).

Using the calculated NMEs in ^{76}Ge , together with the measured half-lives: $\tau_{0\nu}(0_1^+) > 1.8 \cdot 10^{26}$ yr [6], and $\tau_{0\nu}(0_2^+) > 7.5 \cdot 10^{23}$ yr [7], and the $G(0_{1,2}^+)$ factors from [54], we get from (31) the lower limits for $\langle m_\nu \rangle$, that are shown in the last column of Table 4.

When compared with the calculation of the $2\nu\beta\beta$ -decay from Table 2, it is observed that the differences between the two results for $0\nu\beta\beta$ NMEs are relatively smaller. On the other hand, as expected both current values of $M^{0\nu}(0_1^+)$ in ^{76}Ge are notably smaller than those obtained in our *pn*-QRPA calculation [30], which was $M^{0\nu^-}(0_1^+) = 3.19_{+0.46}^{-0.24}$.

In the lower part of Table 4 are presented the $0\nu ee$ -capture NMEs for the $\mathcal{J}_f^+ = 0_{1,2}^+$ final states in ^{124}Te , evaluated with 7 and 9 single-particle levels, obtaining quite similar results. In both cases, they are noticeably smaller than our $0\nu\beta\beta^-$ -decay NMEs for ^{76}Se .

4.4 DCE Sum Rules, and Calibration of NMEs

To verify the sum rules (11) we have to evaluate the total reaction strengths $S_{J\mathcal{J}}^{\{\mp 2\}}$ from (8) and (16), and their differences $S_{J\mathcal{J}}^{\{2\}}$ from (11). This will allow us to calibrate the NMEs $M_{J\mathcal{J}}$ from (13). But, to calibrate in the same way the NMEs $M_V^{0\nu}$, and $M_A^{0\nu}$, we also need to know the total and vector and axial vector strengths $S_{V,A}^{0\nu\mp}$, which are calculated from (32), but with $M_V^{0\nu\mp}(0_f)$, and $M_A^{0\nu\mp}(0_f)$ in place of $M^{0\nu\mp}(0_f^+)$.

Table 4 At the top is the comparison between the NMEs $M^{0\nu^-}(0_f^+) \equiv M^{0\nu}$, and $M_{J\mathcal{J}}^-(0_f^+) \equiv M_{J\mathcal{J}}$, for the $0_f^+ = 0_{1,2}^+$ states in ^{76}Se , within the DCEQTDA, with parameterizations P1 and P2. The upper bounds of $\langle m_\nu \rangle$ are evaluated from Eq. (31), and are given in units of eV. In doing so, we have used the measured half-lives: $\tau_{0\nu}(0_1^+) > 1.8 \times 10^{26}$ yr [6], and $\tau_{0\nu}(0_2^+) > 4 \times 10^{23}$ yr [7]. The lower part of the table shows the same but only the NMEs $M^{0\nu^+}(0_f^+) \equiv M^{0\nu}$ for electron capture in the $0_f^+ = 0_{1,2}^+$ states of ^{124}Te , obtained with 7, and 9 single-particle levels. In this case, we do not make the comparison with reaction NMEs. All NMEs are multiplied by 10^3 .

0_f^+	$M_V^{0\nu}$	$M_{V_{0^+,A_{1^+}}}^{0\nu}$	$ M_{00} $	$M_A^{0\nu}$	$M_{A_{1^+}}^{0\nu}$	$ M_{10} $	$M_P^{0\nu}$	$M_M^{0\nu}$	$M^{0\nu}$	$\langle m_\nu \rangle$
^{76}Se										
P1										
0_1^+	234	145	221	946	466	399	-91	45	1133	0.69
0_2^+	168	106	170	826	457	419	-72	33	955	60.9
P2										
0_1^+	-296	-198	305	-1176	-650	573	105	-50	-1417	0.55
0_2^+	211	144	234	1030	635	594	-82	36	1195	48.6
^{124}Te										
7 levels										
0_1^+	34			133			-14	8.0	162	
0_2^+	5.7			6.8			-3.4	1.0	10	
9 levels										
0_1^+	42.9			142			-15	8.4	178	
0_2^+	-9.3			-5.2			-3.0	-0.9	-12	

All results for the DCE transition strengths in ^{76}Ge , and ^{124}Xe are summarized in Table 5. We also show results for the partial vector and axial-vector strengths $S_{V_{0^+,A_{1^+}}}^{0\nu^\mp}$, which were defined in Section 4.3.1.

We have found that:

1) In the case of ^{76}Ge , identical results are obtained with parameterizations P1 and P2.

2) In the case of ^{124}Xe , both calculations with 7 and 9 single-particle states satisfy the sum rules (11).

3) To satisfy the conditions in Eq. (12), it is essential to include the term $2S_1^{\{-1\}}$ in (11); otherwise, for example, in ^{76}Ge , instead of $S_{10}^{\{2\}} = 353$, we obtain $S_{10}^{\{2\}} = 312$.

4) Since $S_{J\mathcal{J}}^{\{2\}}$ are independent of the nuclear model, and as the term proportional to C is not taken into account when evaluating $S_{10}^{\{2\}}$, and $S_{12}^{\{2\}}$, the result:

$$S_{00}^{\{2\}} \cong S_{00}^{\{2\}}, \quad S_{10}^{\{2\}} \geq S_{10}^{\{2\}}, \quad S_{12}^{\{2\}} \leq S_{12}^{\{2\}},$$

implies that are satisfied both the DCER sum rules (11), and the relations (12). This, in turn, means that the reaction transition strengths $S_{J\mathcal{J}}^{\{-2\}}$, and $S_{J\mathcal{J}}^{\{+2\}}$ are evaluated correctly. Then, it is reasonable to assume that the results for the total transition strengths $S_{V,A}^{0\nu^\mp}$, and $S_{V_{0^+,A_{1^+}}}^{0\nu^\mp}$ are also correct.

Table 5 Results for the DCER strengths $S_{J\mathcal{J}}^{\{\mp 2\}}$, and the $0\nu\beta\beta^\mp$ -decay strengths $S_{V,A}^{0\nu\mp}$, and $S_{V_0^+,A_1^+}^{0\nu\mp}$, in ^{76}Ge , and ^{124}Xe . In the case of ^{76}Ge identical results are obtained with parameterizations P1 and P2. The inequalities in this table are due to the fact that the C terms in (11) are not included in the calculations.

$J\mathcal{J}$	$S_{J\mathcal{J}}^{\{-2\}}$	$S_{J\mathcal{J}}^{\{+2\}}$	$S_{J\mathcal{J}}^{\{2\}}$	$S_{J\mathcal{J}}^{\{2\}}$	$S_{V,A}^{0\nu-}$	$S_{V_0^+,A_1^+}^{0\nu-}$	$S_{V,A}^{0\nu+}$	$S_{V_0^+,A_1^+}^{0\nu+}$
^{76}Ge								
00	300	0.56	299	264	135	128	1.9	0.23
10	330	1.4	328	≤ 353	469	375	36	1.6
12	1536	6.7	1529	≥ 1403				
^{124}Xe								
					7 levels			
00	549	1.5	548	480	221	217	2.3	0.55
10	641	6.7	634	≤ 661	753	673	43	7.0
12	2996	31.0	2965	≥ 2827				
					9 levels			
00	558	2.0	556	480	231	220	3.3	0.71
10	653	8.0	645	≤ 672	826	685	57	8.1

5) As the term proportional to C is not taken into account when evaluating $S_{10}^{\{2\}}$, and $S_{12}^{\{2\}}$ using (11), the inequalities (12) are satisfied as expected.

6) While the partial strengths $S_{V_0^+,A_1^+}^{0\nu-}$ are only slightly smaller than the total strengths $S_{V,A}^{0\nu-}$, the partial strengths $S_{V_0^+,A_1^+}^{0\nu+}$ are very small compared to the total strengths $S_{V,A}^{0\nu+}$. In both cases the partial strengths $S_{V_0^+,A_1^+}^{0\nu\mp}$ are similar in magnitude to their reaction counterparts $S_{J_0}^{\{\mp 2\}}$. In particular,

$$S_{10}^{\{\mp 2\}} \cong S_{A_1^+}^{0\nu\mp},$$

which is consistent with $|M_{10}| \cong |M_{A_1^+}^{0\nu}|$ reported earlier in Table 4. That is, the total transition strengths of the double Gamow-Teller NMEs are congruent to those of the 0ν axial-vector NMEs that are engendered from the 1^+ intermediate states (see also the Fig. 2).

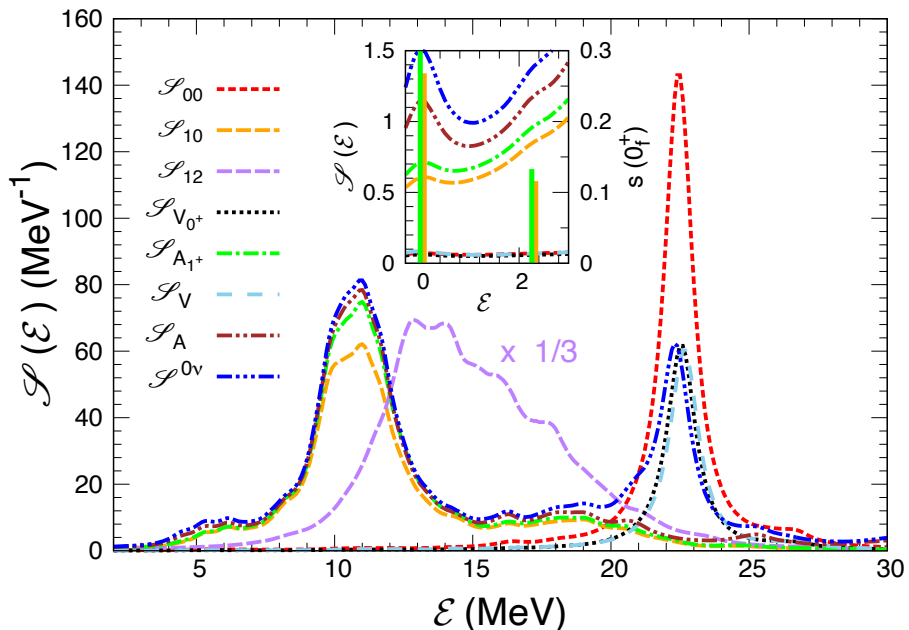
7) From the above results we can now calibrate the NMEs, evaluating the amounts of the total strengths that are concentrated in the ground state, which are defined in Eqs. (13) and (33).

They are shown in Table 6 for ^{76}Ge . All ratios R are of the order of $10^{-4} - 10^{-3}$. These results are fully consistent with the findings of Auerbach *et al.* [3–5], who concluded, from the shell-model study of the $2\nu\beta\beta^-$ -decay in ^{48}Ca , that for the double Gamow-Teller is $R_{10}^-(0_1^+) \sim (10^{-4} - 10^{-3})$.

The above ratios are even smaller in $0\nu ee$ -capture processes. For instance, for the ground state in ^{124}Te with 7 levels we get $R^{0\nu} = 6.9 \cdot 10^{-4}$.

Table 6 Values of the ratios of the strengths defined in (13) for the ground state in ^{76}Se , using the parametrizations P1 and P2. All the ratios are multiplied by 10^3 .

	R_{00}^-	R_{10}^-	$R_V^{0\nu}$	$R_A^{0\nu}$	$R^{0\nu}$
P1	0.29	0.99	6.4	2.9	2.1
P2	0.18	0.66	4.1	1.9	3.3


Fig. 4 The folded strength distributions $\mathcal{S}^{\{-2\}}$ for the DCER and the $0\nu\beta\beta^-$ -decay are shown as a function of the excitation energy \mathcal{E} in the final nucleus ^{76}Se . The intensities $s_{10}^{\{-2\}}$, $s_{A_{1+}}^{0\nu-}$, and $s^{0\nu-}$ of the $0_{1,2}^+$ states are shown in the inset plot.

4.5 DCE Giant Resonances

The comparison made in Table 4 between NMEs is now extended to the full strength distributions of the $0\nu\beta\beta$ -decay and DCER NMEs, plotting their squares as a function of the excitation energies \mathcal{E}_f . Thus, we show in Figure 4 the folded transition densities \mathcal{S} , defined in (34), for the strengths $s_{00}, s_{10}, s_{12}, s_{V_{0+}}^{0\nu-}, s_{V_{0+}}^{0\nu-}, s_{A_{1+}}^{0\nu-}, s_A^{0\nu-}$, and $s^{0\nu-}$ in ^{76}Ge , using the parametrization P2.

From this figure it is clear note that the densities $\mathcal{S}_{00}^{\{-2\}}$ and $\mathcal{S}_V^{0\nu-} \cong \mathcal{S}_{V_{0+}}^{0\nu-}$ behave similarly to each other, as do $\mathcal{S}_{10}^{\{-2\}}$ and $\mathcal{S}_A^{0\nu-} \cong \mathcal{S}_{A_{1+}}^{0\nu-}$. They are concentrated, respectively, at ~ 21 MeV, and at ~ 13 MeV, where the corresponding DCE resonances, *i.e.*, the Double Isobaric Analog State (DIAS), and the Double Monopole Gamow-Teller Resonance (DMGTR), are localized.

Our DCETDA result for DIAS energy agrees well with the analytical estimate by Roca-Maza, Sagawa and Colò [78] given by

$$\mathcal{E}_{DIAS} = 2\mathcal{E}_{IAS} + \Delta\mathcal{E}_{Coul}, \quad (56)$$

where E_{IAS} is the energy of the isobaric analog state (IAS), defined as

$$\mathcal{E}_{IAS} = \mathcal{E}_{Coul}(Z, A) - \mathcal{E}_{Coul}(Z, A - 1). \quad (57)$$

The Coulomb energies are taken from [79, (2-19)], *i.e.*,

$$\mathcal{E}_{Coul}(Z, A) = 0.70 \frac{Z^2}{A^{1/3}} [1 - 0.76Z^{-2/3}] \text{ MeV}, \quad (58)$$

while from [78, (19)]

$$\Delta\mathcal{E}_{Coul} \cong \frac{3}{2} A^{-1/3} \text{ MeV}. \quad (59)$$

From Eq. (56) we now obtain $\mathcal{E}_{DIAS} = 2 \times 10.21 + 0.35 \text{ MeV} = 20.77 \text{ MeV}$, which agrees perfectly with our nuclear model calculations, given in Fig. 4 by the peak energy of $\mathcal{S}_{00}^{\{-2\}}$.

Also shown in the same figure the DCER quadrupole strength $\mathcal{S}_{12}^{\{-2\}}$, and its double quadrupole Gamow-Teller resonance (DQGTR) at $\sim 14 \text{ MeV}$. As mentioned above, this resonance is not related to the Majorana mass. However, the comparison between calculations and experimental data are important to test the nuclear models.

The total density distribution $\mathcal{S}^{0\nu^-}$ is the envelope of $\mathcal{S}_V^{0\nu^-}$, and $\mathcal{S}_A^{0\nu^-}$, including also the pseudoscalar and weak magnetism contributions. Very similar spectra are obtained when the parameterization P1 is used, with the main differences being: (i) the axial vector strength now peaks at $\sim 15 \text{ MeV}$, and (ii) the insertion plot is modified somewhat, as indicated in Table 4.

Needless to say, only the NMEs that are within the Q -value window (shown in the inset of Figure 3), are significant to the neutrino mass. It is relevant to note in this insert the similarity of $s_{10}^{\{-2\}}$ with $s_{A_{1+}}^{0\nu^-}$ and its difference with $s_{0\nu^-}$. Of course, the same issue can be seen in Table 3.

However, the entire reaction spectrum ($\mathcal{S}_{00}^{\{-2\}} + \mathcal{S}_{10}^{\{-2\}}$) can, in principle, be measured, and especially in the region of DIAS, and DMGTR resonances, which are well separated from each other. It would then be worthwhile to perform such a measurement, and compare the resulting data with theoretical predictions, in line with what was done in Ref. [80] for the two GT spectra $\mathcal{S}_{10}^{\{\mp 1\}}$ in ^{48}Sc , and in Ref. [81] for the GT spectrum $\mathcal{S}_{10}^{\{-1\}}$ in ^{132}Sb . Agreement between such measurements with the calculations shown in Fig. 4 them would test our nuclear structure model, as well as that the predictions about the NMEs make sense.

4.6 Relationships between calculations and reaction data

The question posed here is whether the DCE transition strengths $\mathcal{S}_{JJ}^{\{\pm 2\}}$ are experimentally accessible, in the same way as the SCE strengths $\mathcal{S}_{10}^{\{\pm 1\}}$ [80, 81] are ?

It should be recalled that in the SCE case it is possible to study GT transitions via light-ion-induced reactions, such as (n,p), (p,n), (^3He ,t), and (t, ^3He), thanks to the proportionality relationship between the zero angular momentum transfer cross section, σ (at a forward angle) and the corresponding GT strength $s_1^{\{-1\}}$ (see [80, Eq. (3)], and [81, Eq. (1)]). Namely,

$$\sigma_{SCE-GT} \sim \mathcal{S}_1^{\{-1\}}, \quad (60)$$

where the strength density $\mathcal{S}_1^{\{-1\}}$ in the odd-odd nucleus is defined in the same way as $\mathcal{S}_{JJ}^{\{-2\}}$ in Eq. (38) for the final nucleus, with $s_J^{\{\mp 1\}}(J_i)$ instead of $s_{JJ}^{\{\mp 2\}}(J_f)$.

In the DCE case happens something similar in the (π^+ , π^-) reactions, but only with Fermi transitions, for which

$$\sigma_{DCE-F} \sim S_{00}^{\{2\}} \cong S_{00}^{\{-2\}}, \quad (61)$$

as demonstrated in [82, Fig. 1] (see also [83]). Moreover, in the spectrum $\mathcal{S}_{00}(\mathcal{E})$, the DIAS resonance is clearly perceived at the energy \mathcal{E}_{DIAS} , given by Eq. (56), as can be seen in [84, Fig. 2]. Moreover, the Fig. 4 shows that the DIAS is a rather narrow resonance in the Fermi spectra $\mathcal{S}_{00}(\mathcal{E})$, suggesting that near its maximum at \mathcal{E}_{DIAS} , it behaves like

$$\sigma_{DCE-F} \sim \mathcal{S}_{00}^{\{-2\}}(\mathcal{E}). \quad (62)$$

The pion, however, interacts weakly with states involving the spin degree of freedom and therefore states such as DMGTR and DQGTR are not observed in (π^+ , π^-) reactions.

As mentioned above, heavy ion DCE reactions are being carried out using light ions such as ^{18}O . It is hoped to learn something about the magnitude of the $0\nu\beta\beta$ NMEs by measuring the M_{00} , and M_{10} , whose weak analogs $M_{V_{0+}}^{0\nu}$, and $M_{A_{1+}}^{0\nu}$ are the major contributor to them, as seen in Table 4, and discussed in detail above.

The difficulty is due these heavy ion DCE reactions are much more complicated than those of (π^+ , π^-), especially since they probe the NMEs of the projectile and the target at the same time, requiring additional theoretical efforts to disentangle the two types of contributions [9, 21, 85]. In this scenario, the Gawow-Teller cross section cannot be expressed in the form of the Fermi cross section, given by Eq. (61).

Based on a previous work of Bertulani [86], Santopinto *et al.* [16] have recently reported that, for the ground-state target nuclei the DCE differential

cross section within the low-momentum-transfer limit can be factored into: i) a reaction part, which is computed by means of the eikonal approximation, and ii) the nuclear part

$$\mathcal{N} = \left| \frac{M_{00}^P M_{00}^T}{\bar{E}_0^P + \bar{E}_0^T} + \frac{M_{10}^P M_{10}^T}{\bar{E}_1^P + \bar{E}_1^T} \right|^2, \quad (63)$$

where P and T stand for projectile and target nuclei respectively, and

$$\bar{E}_J = \frac{\sum_i s_J^{\{-1\}}(J_i)(E_{J_i}^{\{-1\}} - E_{0^+}^{\{0\}})}{S_J^{\{-1\}}} \quad (64)$$

are the averaged energies of the intermediate nucleus (see (1)). The purpose is to put an upper limit on M_{10}^T , which will correspond to an upper limit on $M^{0\nu}$ for $\beta\beta$ -decaying nuclei. Something similar has been done previously by Cappuzzello *et al.* [21] for the reaction $^{40}\text{Ca}(^{18}\text{O}, ^{18}\text{Ne})^{40}\text{Ar}$, in which the $\beta\beta$ -decay does not occur.

All NMEs and energies in (63) can be calculated straightforward in the DCEQTDA, and we only need the experimental values of \mathcal{N} to make the comparison with the data. This would be the first step toward the calibration of $M^{0\nu}$ by heavy ion reaction experiments.

Finally, it should be noted that only at low momentum transfer are the NMEs in heavy-ion reactions of the form of Eq. (16), where only the intermediate $J^\pi = 0^+, 1^+$ states contribute, as in $2\nu\beta\beta$ -decay. In fact, as pointed out in Ref. [85], the transition amplitude requires in the general case the inclusion of all multipole terms with $J^\pi = 0^\pm, 1^\pm, \dots, 10^\pm$, since the momentum transferred is of the order of $q \geq 400$ MeV/c as in the $0\nu\beta\beta$ decay, where $q \sim 100$ MeV/c [87].

5 Summary and Final Remarks

In Section 1 we briefly state that our main goal is to assist the detection of the Majorana neutrino by observing $0\nu\beta\beta$ -decay, which will allow us to find the effective mass of the neutrino $\langle m_\nu \rangle$, provided we know the nuclear matrix element $M^{0\nu}$.

In Section 2 we present the general formalism for the theoretical description of DCE processes described by two-body DCE operators.

In Section 3 we complete the formulation of the DCEQTDA, which was proposed some time ago [47], and developed in detail for application to the $2\nu\beta\beta$ -decay [30]. Here, we extend it to the $0\nu\beta\beta$ -decay.

In Section 4 we use the DCEQTDA formalism to describe different DCE observables, with special emphasis on the ^{76}Ge , and ^{124}Xe . First, in Section 4.2 we study all the DCE observables that have been measured so far, both the static ones (excitation energies in the final nuclei, and the $Q_{\beta\beta^-}$ and Q_{ee} values), and the dynamic ones which are the $\tau_{2\nu}$ half-lives of all 0^+ and 2^+

states that lie within the windows of Q -values, obtaining good agreement with the experimental data for all of them.

After ensuring in this way the reasonableness of the DCEQTDA, we use it in Section 4.3 to study the $0\nu\beta\beta$ -decays and $0\nu ee$ -captures in a series of nuclei. We start in Section 4.3.1 with the analysis of the genesis of the $0\nu\beta\beta$ -decay going to the ground state in ^{76}Se , comparing it with the results of the pn -QRPA. We find that these two nuclear models are physically very different and that the main reason for this is the approximation $\langle \mathcal{J}_f^+ || \mathcal{O}_J^\pm || J_i^+ \rangle \cong \langle \bar{J}_i^+ || \mathcal{O}_J^\mp || \bar{0}^+ \rangle$ performed in the pn -QRPA, as discussed in Section 3.

In section 4.3.2 we make a detailed comparison between the pn -QRPA and DCEQTDA calculations for the $0\nu\beta\beta$, and $0\nu ee$ NMEs of the final ground state. In the same figure, we also show the results of several other theoretical studies, observing that in DCEQTDA the matrix elements turn out to be significantly smaller than in other nuclear models, with the exception of Ab initio models.

In Section 4.3.3 we point out that it is not correct to associate the reaction NMEs M_{00} and M_{10} with the $0\nu\beta\beta$ NMEs $M_V^{0\nu}$, and $M_A^{0\nu}$, as is often done.

In Section 4.4 we have calculated total strengths $S_{J\mathcal{J}}^{\{\mp 2\}}$ in ^{76}Ge , and ^{124}Xe . So far, this has been done only for light nuclei up to ^{48}Ca [4, 14]. To calibrate the $0\nu\beta\beta$ NMEs we have also done so for the total strengths $S_{V,A}^{0\nu\mp}$, which has never been done before. We conclude that the fractions of $S_{J\mathcal{J}}^{\{\mp 2\}}$ and $S_{V,A}^{0\nu\mp}$ are of the order of $10^{-4} - 10^{-3}$ in $0\nu\beta\beta$ -decays and still smaller in $0\nu ee$ -capture processes.

The comparison made in Table 4 between reaction and $0\nu\beta\beta$ NMEs is extended in Section 4.5 by exposing in Fig. 4 the full spectral densities $\mathcal{S}_{J\mathcal{J}}^{\{-2\}}$, and $\mathcal{S}_{V,A}^{0\nu-}$, which also include the giant DCE resonances. The fact that they turned out to be of the same order came as a surprise, as we have found no physical reason to justify it.

We have advanced to the energy region where giant DCE resonances should be found, aware that $\beta\beta$ -decays cannot occur there. However, experimental verification of our prediction would reinforce confidence in the theoretical comparison made.

Although the main motive of this work has been the study of $\beta\beta$ -decays, and in particular of the 0ν -mode, in Section 4.6 we also briefly discuss nuclear reaction experiments, which are related to this decay mode.

We demonstrate that theoretical methods are at hand, ready to describe the DCE reaction data at low momentum transfer that will be available in the near future.

The present nuclear structure model contains the same free parameters as the pn -QRPA model and is specially designed to describe double charge exchange processes. As such it has the following features:

- 1) It calculates the wave functions in the final nuclei, which contains four-quasiparticle excitations and the Pauli Principle, among them, which play a crucial role,

2) It allows working with a single-particle space large enough for the DCE sum rules to be satisfied; and

3) it jointly describes the $\beta\beta$ -decays and DCERs to all 0^+ and 2^+ final states, as well as their Q -values, energies, resonances, and sum rules.

We believe that these three aspects are indispensable for a reliable assessment of $0\nu\beta\beta$ NMEs. The commonly used pn -QRPA model, being limited to the description of ground-state NMEs, does not meet these conditions. As far as we know, the only other nuclear model capable of evaluating all the double charge exchange observables, which we discuss here, is the Shell Model, but such a comprehensive study has not been done. So far, only Auerbach and his collaborators [2–5, 83, 84] have gone in this direction.

Acknowledgments

We sincerely thank Wayne Seale for the careful and enlightening reading of the manuscript. This work was financed in part by the Coordenação de Aperfeiçoamento de Pessoal de Nível Superior Brasil Finance Code 001. A.R.S. acknowledges the financial support of UESC (SEI 073.6766.2020.0010299-61) and Fundação de Amparo à Pesquisa do Estado da Bahia TO PIE013/2016. V. dos S. F. acknowledges the financial support of UESC-PROBOL program.

A Appendix

Table 7 Comparison of the DCEQTDA calculations to data for the $2\nu\beta\beta$ NMEs, and the DCE Q -values $Q_{\beta\beta}$, and Q_{ee} in nuclei: ^{48}Ca , ^{82}Se , ^{96}Zr , ^{100}Mo , ^{116}Cd , ^{128}Te , ^{130}Te , ^{146}Xe , ^{150}Nd , ^{78}Kr , and ^{130}Ba . The experimental values of $M^{2\nu}$ correspond to the G factors from Ref. [60].

Nucleus	\mathcal{J}_f^+	$M^{2\nu}$		$Q_{\beta\beta}$		Q_{ee}	
		cal	exp	cal	exp	cal	exp
^{48}Ca	0_1^+	0.107	0.038	4.016	4.268	-17.383	-21.900
^{82}Se	0_1^+	0.031	0.085	2.155	2.997	-10.459	-12.178
^{96}Zr	0_1^+	0.134	0.080	2.537	3.356	-8.939	-12.516
^{100}Mo	0_1^+	0.084	0.210	0.918	3.034	-9.117	-9.816
	0_2^+	0.599	0.151	—	—	—	—
^{116}Cd	0_1^+	0.030	0.108	1.322	2.813	-8.969	-8.882
^{128}Te	0_1^+	0.040	0.045	-1.101	2.813	-7.107	-8.881
^{130}Te	0_1^+	0.040	0.030	0.447	2.527	-6.389	-7.221
^{146}Xe	0_1^+	0.024	0.018	1.147	2.457	-9.555	-12.003
^{150}Nd	0_1^+	0.041	0.045	3.406	3.371	-9.290	-8.833
	0_2^+	0.033	0.071	—	—	—	—
^{78}Kr	0_1^+	0.031	0.358	-13.484	-11.004	5.181	2.848
^{130}Ba	0_1^+	0.039	0.175	-9.399	-7.840	4.726	2.619

Table 7 compares the DCEQTDA calculations with the experimental data for the $2\nu\beta\beta$ NMEs, and for the DCE Q -values $Q_{\beta\beta}$, and Q_{ee} , in nuclei other than ^{76}Ge , and ^{124}Xe . In the calculation we have used 9 single-particle levels

in all nuclei except ^{48}Ca , where 7 levels were used. The singlet and triplet coupling constants of the delta force are those of parameterization P1, *i.e.*, $s = s_{sym} = 1$, and $t = t_{sym} \gtrsim 1$.

As indicated in Eq. (31) the experimental NMEs $M^{2\nu}$ depends on both the measured half-life $\tau^{2\nu}$, and the calculated kinematical factor $G^{2\nu}$. The values of $M^{2\nu}(exp)$ listed in Table 7 correspond to the G factors from Ref.[60]. Note that our $M^{2\nu}(exp)$ is in agreement with the M^{eff} of [59].

From the last table it is clear that the agreement between the calculations and the experimental data is quite satisfactory for both NMEs and Q -values, especially if one takes into account that the parameters of the nuclear model were not varied. Indeed, except for ^{100}Mo , ^{78}Kr , and ^{130}Ba , the calculated and measured NMEs are quite close to each other. It is also important that the values of $Q_{\beta\beta}$, both calculated and experimental, are both positive in nuclei decaying by $\beta\beta$, except at ^{128}Te , and negative in nuclei where ee capture occurs. The opposite is true in all cases with Q_{ee} .

References

- [1] C. Brase, J. Menéndez, E. A. Coello Pérez, and A. Schwenk, arXiv:2108.11805v1 [nucl-th].
- [2] D. C. Zheng, L. Zamick, and N. Auerbach, Phys. Rev. C **40**, 936 (1989).
- [3] N. Auerbach, L. Zamick, D.C. Zheng, Annals of Phys. **192**, 77 (1989).
- [4] N. Auerbach, and Bui MinhLoc, Phys. Rev. C **98**, 064301 (2018).
- [5] N. Auerbach, in Journal of Physics: Conference Series (IOP Publishing, 2018), vol. 1023, p. 012032.
- [6] M. Agostini *et al.* (GERDA Collaboration), Phys. Rev. Lett. **125**, 252502 (2020).
- [7] I. J. Arnquist *et al.* (Majorana Collaboration), Phys. Rev. C **103**, 015501 (2021).
- [8] S. Calgareo *et al.* (LEGEND Collaboration), Il Nuovo Cimento 47 C (2024) 69.
- [9] H. Lenske, F. Cappuzzello, M. Cavallaro, and M. Colonna, Prog. Part. Nucl. Phys. **109**, 103716 (2019).
- [10] M. Cavallaro, L. Acosta, P. Adsley, C. Agodi, C. Altana *et al.*, J. Phys. Conf. Ser. **1610**, 012004 (2020).
- [11] P. Finocchiaro *et al.*, for the Numen Collaboration, Universe **6** (9), 129 (2020).

- [12] C. Agodi, F. Cappuzzello, L. Acosta, C. Altana, P. Amador-Valenzuela *et al.*, JPS Conf. Proc. **32**, 010045 (2020).
- [13] F. Cappuzzello, M. Cavallaro, Universe **6** (11), 217 (2020).
- [14] N. Shimizu, J. Menéndez, and K. Yako, Phys. Rev. Lett. **120**, 142502 (2018).
- [15] J. Menéndez, N. Shimizu, and K. Yako, J. Phys. Conf. Ser. **1056**, 012037 (2018).
- [16] E. Santopinto, H. García-Tecocoatzi, R. I. Magaña Vsevolodovna, and J. Ferretti, (NUMEN Collaboration), Phys. Rev. C **98**, 061601(R) (2018).
- [17] E. Santopinto, J. Ferretti, H. García-Tecocoatzi, R.I. Magana Vsevolodovna, within the NUMEN project, J. Phys. Conf. Ser. **1610**, 012013 (2020).
- [18] E. Aprile *et al.*, Nature **568** (2019).
- [19] K. Hiraide *et al.* (XMASS Collaboration), in J. Phys. Conf. Ser. **1342** (IOP Publishing), 1342, 012027 (2020).
- [20] M. Doi, Prog. Theor. Phys. **89**, 139 (1993).
- [21] F. Cappuzzello *et al.*, Eur. Phys. J. A **51**, 145 (2015).
- [22] F. Krmpotić, and S. Shelly Sharma, Nucl. Phys. A **572**, 329 (1994).
- [23] K. Ikeda, S. Fujii, and J. I. Fujita, Phys. Lett. **3**, 271 (1963).
- [24] P. Vogel, M. Ericson, and J. D. Vergados, Phys. Lett. B **212**, 259 (1988).
- [25] K. Muto, Phys. Lett. B **277**, 13 (1992).
- [26] C. Barbero, F. Krmpotić, and D. Tadić, Nucl. Phys. A **628**, 170 (1998).
- [27] T. Tomoda, Phys. Lett. B **474**, 245 (2000).
- [28] R. A. Sen'kov and M. Horoi, Phys. Rev. C **88**, 064312 (2013).
- [29] C. Barbero, F. Krmpotić, A. Mariano, and D. Tadić, Nucl. Phys. A **650**, 485 (1999).
- [30] V. dos S. Ferreira, F. Krmpotić, C.A. Barbero, A.R. Samana, Phys. Rev. C **96**, 044322 (2017).
- [31] J. Beringer *et al.* (Particle Data Group), Phys. Rev. D **86**, 010001 (2012).

- [32] J. D. Walecka, *Theoretical nuclear and subnuclear physics* (World Scientific Publishing Company, 2004).
- [33] F. Šimković, G. Pantis, J. D. Vergados and A. Faessler, *Phys. Rev. C* **60**, 055502 (1999).
- [34] J. M. Yao, L. S. Song, K. Hagino, P. Ring, and J. Meng, *Phys. Rev. C* **91**, 024316 (2015).
- [35] F. Krmpotić, J. Hirsch and H. Dias, *Nucl. Phys. A* **542**, 85 (1992).
- [36] V. dos S. Ferreira, A.R. Samana, F. Krmpotić, and M. Chiapparini, *Phys. Rev. C* **101**, 044314 (2020).
- [37] L. Jokiniemi, J. Menéndez, *Phys. Rev. C* **107**, 044316 (2023).
- [38] J. A. Halbleib and R. A. Sorensen, *Nucl. Phys. A* **98**, 542 (1967).
- [39] P. Vogel and M. R. Zirnbauer, *Phys. Rev. Lett* **57**, 3148 (1986).
- [40] O. Civitarese, A. Faessler and T. Tomoda, *Phys. Lett. B* **194**, 11 (1987).
- [41] T. Tomoda and A. Faessler, *Phys. Lett. B* **199**, 475 (1987).
- [42] J. Engel, P. Vogel and M. R. Zirnbauer, *Phys. Rev. C* **37**, 731 (1988).
- [43] J. Hirsch and F. Krmpotić, *Phys. Rev. C* **41**, 792 (1990).
- [44] J. Hirsch and F. Krmpotić, *Phys. Lett. B* **246**, 5 (1990).
- [45] J. Hirsch, E. Bauer and F. Krmpotić, *Nucl. Phys. A* **516**, 304 (1990).
- [46] A. Staudt, K. Muto, H.V. Klapdor-Kleingrothaus, *Europhys. Lett.* **13**, 31 (1990).
- [47] F. Krmpotić, *Fizika B* **14**, 139 (2005).
- [48] J. Suhonen, *From Nucleons to Nucleus: Concepts of Microscopic Nuclear Theory* (Springer, Berlin, 2007).
- [49] M. K. Pal, Y. K. Gambhir, and Ram Raj, *Phys. Rev.* **155**, 1144 (1966).
<https://doi.org/10.1103/PhysRev.155.1144>
- [50] Ram Raj and M. L. Rustgi, *Phys. Rev.* **178**, 1556 (1969).
- [51] M. Aunola, J. Suhonen, *Nucl. Phys. A* **602**, 133 (1996).
- [52] A. M. Lane, *Nuclear Theory. Pairing force correlations and collective motion*. Benjamin, New York, 1964.

- [53] P. Ring, P. Schuck, *The Nuclear Many-Body Problem*, Springer-Verlag, New York, 1980.
- [54] M. Mirea, T. Pahomi, and S. Stoica, *Rom. Rep. in Phys.* **67**, 872 (2015).
- [55] J. Suhonen, O. Civitarese, *Phys. Rep.* **300**, 123 (1998).
- [56] M. Aunola, J. Suhonen, *Nuc. Phys. A* **602**, 133 (1996).
- [57] B. Pritychenko, National Nuclear Data Center, <http://www.nndc.bnl.gov/> (2011).
- [58] F. Krmpotić, M. N. Rao, O. Sala and A. Szanto de Toledo. *Phys. Rev. C* **16** 438 (1977).
- [59] A. Barabash, *Universe* **6**(10), 159 (2020).
- [60] P. Pirinen and J. Suhonen, *Phys. Rev. C* **91**, 054309 (2015).
- [61] J. Kostensalo, J. Suhonen, K. Zuber, *Phys. Lett. B* **831**, 137170 (2022).
- [62] E. Coello Pérez, J. Menéndez, and A. Schwenk, *Phys. Lett. B* **797**, 134885 (2019).
- [63] O. Civitarese, J. Suhonen, *Phys. Lett. B* **626**, 80 (2005)
- [64] M. Kortelainen and J. Suhonen, *Phys. Rev. C* **76**, 024315 (2007).
- [65] F. Šimkovic, A. Faessler, V. Rodin, P. Vogel, J. Engel, *Phys. Rev. C* **77**, 045503 (2008)
- [66] F. Šimkovic, V. Rodin, A. Faessler, and P. Vogel, *Phys. Rev. C* **87**, 045501 (2013)..
- [67] J. Hyvärinen, J. Suhonen, *Phys. Rev. C* **91**, 024613, (2015).
- [68] J. Jokiniemi, H. Ejiri, D. Frekers, J. Suhonen, *Phys. Rev. C* **98**, 024608 (2018).
- [69] R. A. Sen'kov and M. Horoi, *Phys. Rev. C* **90**, 051301(R) (2014), and R. A. Sen'kov and M. Horoi, *Phys. Rev. C* **93**, 044334 (2016) 4, e-Print: 1512.06157 [nucl-th].
- [70] A. Belley, C. G. Payne, S. R. Stroberg, T. Miyagi, and J. D. Holt, *Phys. Rev. Lett.* **126**, 042502 (2021).
- [71] A. Belley, T. Miyagi, S. R. Stroberg and J. D. Holt, [arXiv:2307.15156 [nucl-th]].

- [72] A. Belley, J. M. Yao, B. Bally, J. Pitcher, J. Engel, H. Hergert, J. D. Holt, T. Miyagi, T. R. Rodriguez, A. M. Romero, S. R. Stroberg and X. Zhang, Phys. Rev. Lett. **132**, 182502 (2024).
- [73] J. Barea, J. Kotila, and F. Iachello, Phys. Rev. C **87**, 057301 (2013).
- [74] J. Barea, J. Kotila and F. Iachello, Phys. Rev. C **87**, 014315 (2013).
- [75] N. L. Vaquero, T. R. Rodríguez and J. L. Egido, Phys. Rev. Lett. **111**, 142501 (2013).
- [76] L.S. Song, J.M. Yao, P. Ring, J. Meng, Phys. Rev. C **90**, 054309 (2014).
- [77] J. Menéndez, A. Poves, E. Caurier and F. Nowacki, D, Nucl. Phys. A **818**, 139 (2009).
- [78] X. Roca-Maza, H. Sagawa, G. Colo, Phys. Rev. C **101**, 014320 (2020).
- [79] A. Bohr and B.R. Mottelson, *Nuclear Structure, Vol. 1* (W. A. Benjamin, New York, Amsterdam, 78, 1969).
- [80] K. Yako, Phys. Rev. Lett. **103**, 012503 (2009).
- [81] J. Yasuda, M. Sasano, R.G.T. Zegers, H. Baba, D. Bazin et al. Phys. Rev. Lett. **121** 13, 132501 (2018).
- [82] M. Kaletka, K. K. Seth, A. Saha *et al.*, Phys. Lett. B **199**, 336 (1987).
- [83] N. Auerbach, W.R. Gibbs, E. Piasezky, Phys. Rev. Lett. **59**, 1076 (1987).
- [84] N. Auerbach, Ann. Phys. **197**, 376395 (1990).
- [85] J. I. Bellone, M. Colonna, J. A. Lay, and H. Lenske (NUMEN Collaboration), Phys. Lett. B **807**, 135528 (2020).
- [86] C. A. Bertulani, Nucl. Phys. A **554**, 493 (1993).
- [87] T. Tomoda, Rep. Prog. Phys. **54**, 53 (1991).